TU Delft

Delft University of Technology

Document Version
Final published version

Licence
CC BY

Citation (APA)
Jones, S. A., Kahrobaei, S., Groenenboom, J., Rossen, W. R., Voskov, D., & Farajzadeh, R. (2026). The Behavior of N_2 and CO_2 Foams under Varying Pressure Conditions. *Energy and Fuels*, *40*(39), 21742-21758. https://doi.org/10.1021/acs.energyfuels.6c02931

Important note
To cite this publication, please use the final published version (if applicable).
Please check the document version above.

Copyright
In case the licence states “Dutch Copyright Act (Article 25fa)”, this publication was made available Green Open Access via the TU Delft Institutional Repository pursuant to Dutch Copyright Act (Article 25fa, the Taverne amendment). This provision does not affect copyright ownership.
Unless copyright is transferred by contract or statute, it remains with the copyright holder.

Sharing and reuse
Other than for strictly personal use, it is not permitted to download, forward or distribute the text or part of it, without the consent of the author(s) and/or copyright holder(s), unless the work is under an open content license such as Creative Commons.

Takedown policy
Please contact us and provide details if you believe this document breaches copyrights.
We will remove access to the work immediately and investigate your claim.

This work is downloaded from Delft University of Technology.

energy&fuels

Open Access

This article is licensed under CC-BY 4.0

pubs.acs.org/EF

Article

The Behavior of N_2 and CO_2 Foams under Varying Pressure Conditions

Siân A. Jones,* Siavash Kahrobaei, Jeroen Groenenboom, William R. Rossen, Denis Voskov, and Rouhi Farajzadeh

Cite This: *Energy Fuels* 2026, 40, 21742−21758

Read Online

ACCESS | Metrics & More | Article Recommendations | Supporting Information

ABSTRACT: Knowledge of how CO_2 foam behaves when flowing through rock is important for many CO_2 Capture, Utilization and Storage (CCUS) applications. Typically, laboratory foam flow tests are carried out at relatively low pressures as compared to reservoir pressures. However, the possibility of foam behavior changing with pressure introduces uncertainty in results that are extrapolated up to reservoir pressure. The current work consists of a series of coreflood experiments to investigate how system pressure affects the behavior of both nitrogen and CO_2 foams flowing through Bentheimer sandstone. For each gas, the system pressures were varied in steps from 5 bar up to 200 bar, with values of 5, 50, 100, 150, and 200 bar for the nitrogen tests, and 5, 25, 50, 70, 80, 120, 160, and 200 bar for the CO_2 tests. Foam-quality scans were carried out at each pressure step to provide full data on the foam behavior at each individual pressure. Implicit-texture foam model parameters were then fitted for each pressure step. Two corefloods were also carried out in the CT scanner to determine the water saturations within the core and consider the variation in water saturation S_w with injected foam quality and injected gas type—nitrogen or CO_2. It was found that for nitrogen, the apparent foam viscosity was only weakly affected by pressure, with an increasing pressure giving only a small increase in the maximum apparent viscosity. In contrast, the foam flow behavior of CO_2 changed significantly with pressure, and it is suggested that this variation is linked to four factors that vary strongly with pressure: 1) CO_2 density, 2) the interfacial tension between the CO_2 and the surfactant solution, 3) the effect of CO_2 chemistry on surfactant behavior, and 4) the contact angle of the CO_2 on the rock. These four factors are all pressure-dependent and have the potential to affect foam generation, trapped-gas fraction, and foam stability.

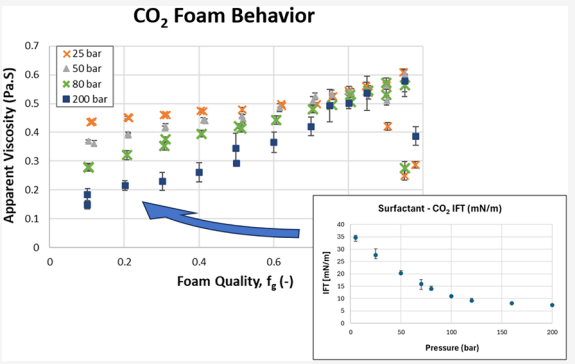

INTRODUCTION

An understanding of CO_2 foam flow behavior through rock is important for many subsurface applications, including carbon capture and storage[1−3] (CCS) as well as foam-enhanced oil recovery[4] (EOR). However, efficient injection of CO_2 depends on an effective combination of both microscopic and macroscopic sweep. CO_2 provides very good microscopic sweep, i.e., at the pore scale, but, for many reservoirs, achieving an efficient macroscopic sweep can be challenging, with thief zones and gravity override affecting the stability of the displacement front. Generating a foam with CO_2 is intended to improve the sweep efficiency and reduce instabilities in the displacement front across the volume of the reservoir.

Because of the potential uses of CO_2 foam, a large body of work had been carried out looking at CO_2 foam behavior in corefloods.[5−7] However, lab tests are often limited in the operational pressures that can be achieved, and these operational pressures tend to be significantly lower than actual reservoir pressures, which can range from 200 bar to >1000 bar.[8]

Previous work has been carried out to consider CO_2 foam behavior at elevated pressures, but this usually takes the form of tests carried out at a single high pressure. Examples of such tests include: 1) investigating a small range of foam qualities (0.55−0.85) at 138 bar;[9] 2) full foam quality scans at 138,[10] 145,[11] 175,[12] or 551 bar;[13] 3) SAG injection at 138 bar;[14] and 4) contour plots of pressure gradients as functions of gas and liquid velocities at 103 and 138 bar.[15]

In contrast to the work described in the previous paragraph, some authors[16−18] have considered the effect of varying pressure on foam behavior, but these tests were restricted to examining the behavior of a single foam quality. Aarra et al.[17] tested both nitrogen and CO_2 at 30, 120, and 280 bar, focusing on a foam quality, f_g, of 0.8, and considered how the foam behavior varied with the number of pore volumes (PV) injected. They observed that, while nitrogen showed very little variation in behavior with

Received: June 5, 2026
Revised: September 3, 2026
Accepted: September 4, 2026
Published: September 20, 2026

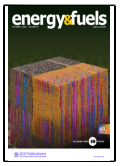

ACS Publications

© 2026 The Authors. Published by American Chemical Society

Downloaded from pubs.acs.org/enfuem/article-pdf/40/39/21742/6856758/acs.energyfuels.6c02931.pdf by TU DELFT user on 12 October 2026

pressure, foam strength with CO_2 decreased dramatically (by a factor of >50) as the system pressure increased from 30 to 280 bar. Solbakken[16,18] extended the range of pressures by including extra tests at 90 bar and again saw a similar reduction in CO_2 foam strength with increasing pressure.

The current authors have been unable to find any published work for CO_2 foam corefloods where the foam quality is varied for a range of system pressures. This comprehensive information on CO_2 foam behavior is required to give a full description of the foam response to pressure and ensure that the data available for the reservoir models is fully reliable. The aim of the current work was, therefore, to investigate how changing the system pressure affects the behavior of CO_2 foams over a wide range of foam qualities. Foam coreflood tests were also carried out with nitrogen at varying pressures to provide a baseline of behavior.

MATERIALS AND METHODS

Surfactants and Brines

An amphoteric surfactant, cocamidopropyl hydroxysultaine (AMPHOSOL CS-50, Stepan), was selected for the foam coreflood tests. This sultaine surfactant had previously been used in a series of CO_2 foam coreflood tests in carbonate rock and had been shown to have good foaming behavior with supercritical CO_2.[19] A 4-salt synthetic seawater, with the composition given in Table 1 and with total dissolved solids (TDS) of 30.20 g/L, was used for all the coreflood tests carried out. Foaming solutions were made with 0.5 wt % active material of the surfactant in the synthetic seawater.

Table 1. Synthetic Seawater Recipe

Salt	Quantity (g/L)
NaCl	28.396
KCl	0.749
$MgCl_2 \cdot 6H_2O$	1.421
$CaCl_2 \cdot 2H_2O$	0.521
TDS	30.204

The surfactant solutions were vacuum-degassed before using, and an oxygen scavenger (100 ppm carbohydrazide) was also added to minimize any oxidation issues at the elevated temperature used during testing.

Rock Samples

All the coreflood tests were carried out using outcrop Bentheimer Sandstone core plugs of diameter 4 cm and length 17 cm. Bentheimer is a homogeneous sandstone with relatively high permeability, ~2D, and the exact permeability (to brine) of each core plug was measured before testing commenced. The porosity of the Bentheimer was measured using a pycnometer and found to have a value of 0.22 ± 0.005.

Experimental Procedures

Coreflood Setups. Two coreflood setups were used for the foam tests: one for the lower-pressure tests (Figure 1) and one for the higher-pressure tests (Figure 2). In both cases, the core was placed horizontally within the oven. For test pressures up to 150 bar, a PEEK core holder could be used, and for test pressures higher than 150 bar, a titanium core holder was used. Before mounting in the core holder, the core plugs were coated with a layer of aluminum-filled epoxy resin (Rencast CW 47, Huntsman) to prevent any bypass of the rock by the injected fluids. A confining pressure, either equal to the inlet pressure (Figure 1) or approximately 5 bar higher (Figure 2), was applied to the outside of the glued core to ensure that there was no resultant effective stress on the core during testing.

For both the setups, the mixing-T, where the injected gas and brine were combined, was placed just outside the oven; then the fluid mixture was passed through an extended coil of tubing inside the oven (~2 m long). This allowed the mixed fluids to equilibrate with each other, as well as coming to temperature, before reaching the core.

Experiment Methodology. All tests were carried out at 60 °C. Nitrogen foam behavior was tested with system pressures (as defined by the back-pressure) of 5, 50, 100, 150, and 200 bar, and CO_2 foam behavior was tested with system pressures of 5, 25, 50, 70, 80, 120, 160, and 200 bar. The extra values of pressure tested with CO_2, as compared to the nitrogen tests, were added to give more detailed information on the foam response to pressure as well as information on foam behavior around the gas-to-supercritical transition of CO_2 (at 74 bar for 60 °C[20]).

For each step in the system pressure, the test was started by fully saturating the core with brine, then measuring the rock's permeability to brine (at the test pressure). Following this, the core was flooded with at least 5 pore volumes (PV) of surfactant solution to fulfill any adsorption of the surfactant to the rock surface. Then co-injection of the gas with the surfactant solution was started, with a total (combined) flow rate of 1 mL/min (equivalent to 1.47×10^{-5} m/s or 4.17 feet/day). A range of foam qualities (f_g) was injected, where

$$f_g = Q_g/(Q_g + Q_l)$$

and Q_g and Q_l are the gas and liquid flow rates, respectively, as defined at the test conditions at the midpoint of the core. To ensure that the Q_g at the midpoint of the core was at the desired value, the gas flow from the mass flow controller, or pump, was adjusted over the course of each test to take into account any variation in the midpoint pressure—for

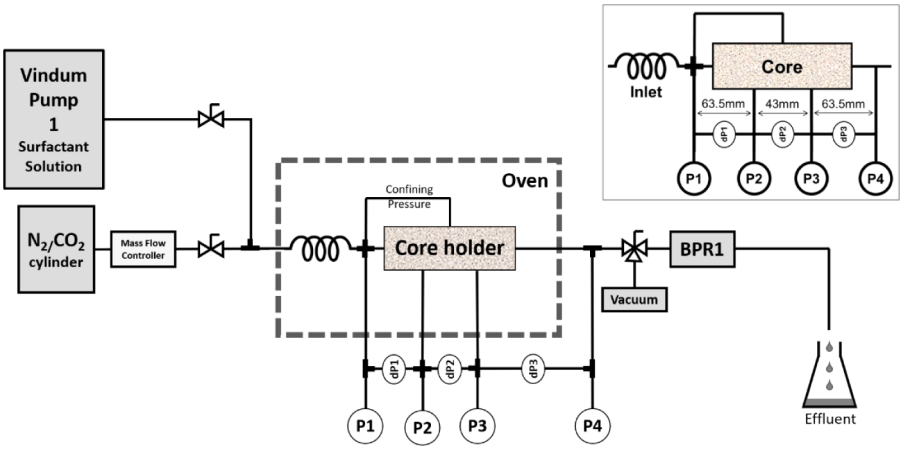

Figure 1. Schematic diagram of the lower-pressure foam-flood setup, used for all the test pressures up to 150 bar. The core-holder in this setup is made from PEEK, and the fittings and connectors are PEEK, Radel, or Monel. The inset shows the positions of the pressure and dP gauges.

https://doi.org/10.1021/acs.energyfuels.6c02931
Energy Fuels 2026, 40, 21742−21758

Downloaded from pubs.acs.org/enfuem/article-pdf/40/39/21742/6856715 8/acs.energyfuels.6c02931.pdf by TU DELFT user on 12 October 2026

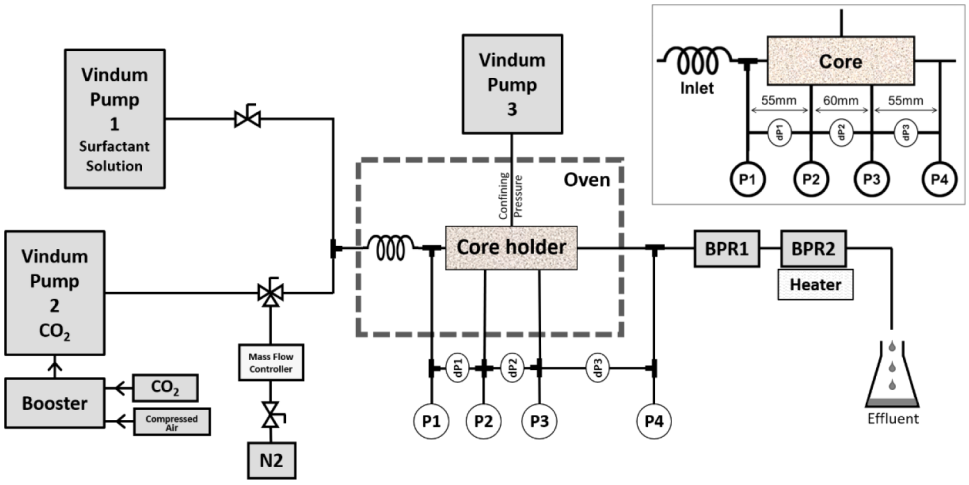

Figure 2. Schematic diagram of the high-pressure foam flood setup, used for test pressures from 160 bar upwards. The core holder in this setup is titanium, and the fittings and connectors are Inconel or Hastelloy. The inset shows the positions of the pressure and dP gauges.

example, when a strong foam was generated that gave a large pressure gradient along the core.

For the tests with CO_2, the solubility of the CO_2 into the injected brine could be significant, and the long spiral inlet tube (Figure 1) was included in the setup to ensure that the CO_2 and brine were in equilibrium with each other before reaching the core. The solubility was taken into account when calculating the required flow rate of CO_2 from the pump, Q_{CO_2-pump}, to give the correct Q_g in the middle core, where

$$Q_{CO_2-pump} = Q_g + Q_{CO_2-lost-to-dissolution} \quad (1)$$

The volume of CO_2 dissolved into the brine, $Q_{CO_2-lost-to-dissolution}$, was extrapolated from the data provided by Duan et al.[21]

For both the nitrogen and CO_2 tests, there was also a difference in fluid density between the pump, or mass flow controller (MFC), at room temperature and the core at 60 °C. This difference in fluid density was particularly significant for the higher-pressure CO_2 tests, where the CO_2 was liquid in the pump and supercritical in the core. To rectify the error in Q_g caused by this density difference, a correction of the gas flow rate set on the pump or MFC was made to take into account any variation in fluid density. An in-depth discussion of all the flow corrections used to give accurate values of Q_g is given in Jones et al.[19]

To avoid any hysteresis effects, the tests were alternated between high and low qualities. At each foam quality, flow was continued until a steady-state pressure drop was achieved along each section of the core, i.e., inlet (dP1), midsection (dP2), and outlet (dP3), as indicated in Figures 1 and 2. The steady-state pressure drop in each section of the core was then used to calculate the apparent viscosity, μ_{app}, of the foam in each section, using Darcy's law:

$$\mu_{app} = \frac{k\nabla P}{u_t} \quad (2)$$

where k is the rock permeability (to brine), u_t ($=u_g + u_l$) is the total superficial velocity (and u_g and u_l are the gas and liquid superficial velocities, respectively), and ∇P is the absolute, average pressure gradient along each section of the core. The gas velocity, u_g, used in this calculation took into account the corrections for solubility (eq 1) and fluid density mentioned above. Due to the large pressure gradients along the core, each section of the core—inlet, midsection, and outlet—was treated separately when carrying out the density and solubility corrections. In each case, the mid-point pressure of the section was used to determine the relevant density or solubility parameter for that section.

Finally, at the end of the test, the core was flushed with 3 to 4 PV of 50:50 IPA/brine solution to kill any foam in the core. The IPA/brine mixture was then flushed from the core by using at least 10 PV of brine. The permeability of the core could then be retested, and a new test started at the next pressure point.

CT Scanner Tests. Two foam-flood tests were carried out in the CT scanner to check on the variation of water saturation during the tests and to confirm the difference between nonfoam and foam behavior. The coreflood setup used was the one shown in Figure 1, but with the oven replaced by a heating jacket coupled with a heated recirculating bath operating in external-circulation mode.

The two foam-flood tests were carried out at 5 bar and a total flow rate of 1 mL/min, with the first test using CO_2 and the second test using nitrogen. In each case, as for the main test series described above, the surfactant solution and gas were co-injected to produce foam near the entrance of the core, and the resultant pressure drops along the core were used to determine the apparent viscosity of the generated foam. One set of "no-foam" measurements was also carried out at the start of the carbon dioxide test sequence by simply co-injecting the 4-salt brine and the CO_2 at three different gas fractions, f_g, of 0.1, 0.5, and 0.9.

The medical CT scanner used for the tests was a dual-source Siemens Somatom Definition scanner. The machine was operated at 140 kV and 250 mAs, with a slice thickness of 0.6 mm along the core. There was a resolution of 0.2 mm in the $x-y$ plane (i.e., transverse slice of the core) when operating with a 10 cm field of view. This gave a voxel size of 0.2 × 0.2 × 0.6 mm. Following reconstruction of the CT image, each voxel was given a value equal to the attenuation coefficient on the Hounsfield scale, HU, of the material in that voxel.

Analysis of the CT images was carried out using ImageJ to determine the water distribution along a longitudinal slice of the core and to calculate the average water saturation as a function of distance from the injection point. To be able to carry out this calculation, scans were first made of both a fully dry core, HU_{dry}, and a fully water-saturated core, HU_{wet}. The water saturation, S_w, could then be calculated using:

$$S_w = \frac{HU_{foam} - HU_{dry}}{HU_{wet} - HU_{dry}}$$

where HU_{foam} is the attenuation coefficient in the presence of foam,[22] with the values of S_w averaged across each transverse slice of the core.

Measurement of Surface Tension and Contact Angles at Coreflood Pressures

A pendant-drop cell was used to carry out both surface-tension and contact-angle measurements. The cell is made of titanium and is capable of operating at pressures up to 200 bar and at high temperatures. This allows measurements to be made at the coreflood temperature (60 °C) and over the full range of pressures used in the coreflood experiments.

For the surface tension measurements, the pendant-bubble technique was used. The cell was initially filled with demineralized water (demiwater) or the surfactant solution; then the pressure was set using a back-pressure regulator. Nitrogen or CO_2 was injected via a

Downloaded from pubs.acs.org/enfuem/article-pdf/40/39/21742/6856715/acs.energyfuels.6c02931.pdf by TU DELFT user on 12 October 2026

https://doi.org/10.1021/acs.energyfuels.6c02931
Energy Fuels 2026, 40, 21742−21758

Table 2. Rock Parameters for Bentheimer Sandstone and Amphoteric Surfactant Used in the Implicit-Texture (STARS) Fitting Script.[a]

	S_{wc}	S_{gr}	n_w	n_g	k_{rw0}	k_{rg0}
	Connate water saturation	Irreducible gas saturation	Corey water exponent	Corey gas exponent	Endpoint water relative permeability	Endpoint gas relative permeability
Nitrogen	0.05	0.03	2.6	2	0.713	0.587
CO_2	0.05	0.04	3.2	2	0.713	0.587

[a] k_{rw0} and k_{rg0} were taken from Eftekhari and Farajzadeh,[22] and the other parameters were obtained from analysis of local CT data (see Figure 16 and Table 6).

capillary tube (1.59 mm ID) at the base of the pendant-drop cell. A video camera was then used to capture the shapes of the rising bubbles. The images obtained were analyzed using OpenDrop, an open-source software package,[23] to determine the surface tension for each gas and at each pressure.

The contact-angle measurements were carried out on a piece of polished quartz crystal, which could be mounted within the pendant-drop cell. The smooth crystal was selected, rather than a Bentheimer sample, to avoid the effects that the rock's surface roughness can have on the measurements.[24] For each measurement, the cell was again filled with demi-water or surfactant solution and pressurized to the test pressure. Small bubbles of CO_2 were injected from the base of the cell to rest against the quartz surface. Photos of the bubbles were taken at regular intervals, and the images were analyzed using a method based on the Young–Laplace equation, as described by Hashemi et al.,[25] to determine the contact angle.

Determination of Implicit-Texture Foam Parameters

An Implicit-Texture (or local equilibrium) foam model such as STARS[26] can be used to effectively model foam behavior for reservoir simulations. As previously described,[27−29] the Implicit-Texture model does not explicitly describe the behavior of the foam but instead focuses on quantifying the reduction in the gas mobility due to the presence of the foam. To do this, the model introduces a nondimensional mobility-reduction factor, *FM*, which can be applied to the gas-phase relative permeability, k_{rg}, to give the gas-phase relative permeability in the presence of foam, k_{rg}^f, i.e.:

$$k_{rg}^f = k_{rg} \cdot FM$$

The value of *FM* can then be defined by the product of up to six other functions, but in the current situation only two functions, F_2 and F_S, were considered:

$$FM = \frac{1}{1 + fmmob \cdot F_2 \cdot F_S}$$

where *fmmob* is the reference mobility factor, F_2 describes the effect of water saturation, and F_S is related to the capillary number, N_{ca}. F_2 and F_S can then be defined in relation to the five Implicit-Texture foam parameters—*fmmob, epdry, fmdry, fmcap*, and *epcap*—as follows:

$$F_2 = 0.5 + \frac{\arctan[epdry \cdot (S_w - fmdry)]}{\pi}$$

where S_w is the water saturation.

$$F_S = \left(\frac{fmcap}{N_{ca}}\right)^{epcap}, \text{ and } N_{ca} = \frac{k\nabla P}{\sigma_{wg}}$$

where σ_{wg} is the gas-water interfacial tension.

The five Implicit-Texture foam parameters could be fitted using a locally available MATLAB script.[30] This process was carried out for all of the data at each pressure step to determine if, and how, the parameters change with pressure. The MATLAB script allows for a full five-parameter fit, which can be carried out with either a least-squares optimization or a constrained optimization, where upper and lower bounds could be put on the parameters to ensure that they remain in a realistic range.

The basic rock and fluid parameters used for the fitting script are given in Table 2. These values were obtained from the work of Eftekhari and Farajzadeh[22] and from analysis of CT data obtained during several of the corefloods (see Figure 16 and Table 6). The upper and lower bounds used for the constrained optimization are given in Table 3. The gas viscosities and interfacial tensions for the CO_2 and nitrogen, required for the fitting script, are given in Tables S1 and S2 (in Supporting Information).

Table 3. Upper and Lower Bounds Used for the Constrained Optimization in the Implicit-Texture Parameter Fitting Script

	fmmob	epdry	fmdry	fmcap	epcap
Upper bound	1e9	2e5	0.4	1e-3	3
Lower bound	1	1	0.05	1e-7	0.01

RESULTS AND DISCUSSION

Surface Tension and Contact Angle Measurements

Measurements of the surface tension were carried out at 60 °C for the surfactant solution with both nitrogen and CO_2. Surface-tension measurements were also carried out with demi-water for the CO_2. The variation in the surface tension with pressure is shown in Figure 3. As expected,[31−37] it was found that increasing the system pressure reduces the surface tension. The nitrogen showed a small, linear decrease with pressure (Figure 3a). The CO_2, however, showed a very strong decrease in surface tension as the pressure increased up to 100 bar (Figure 3b), dropping from ∼35 mN/m at 5 bar to ∼10 mN/m at 100 bar. The decrease was more gradual at pressures >100 bar. The CO_2 showed a similar trend for the demi-water measurements (Figure 3c), with the surface tension dropping more than 20 mN/m as the pressure increased to 100 bar. The shape of the CO_2 curves is likely the result of both CO_2 solubility effects and phase effects,[33] with the increase in CO_2 solubility with pressure correlating with the reduction in surface tension, up to approximately the transition to supercritical.

The contact-angle measurements for the quartz crystal with CO_2 at 60 °C in both the demi-water and the surfactant solution are given in Figure 4a. For the demi-water test, the behavior showed a similar trend to that seen by Ameri et al.,[38] with the contact angle showing very little change at pressures up to ∼50 bar. The contact angle then increased significantly as the pressure continued to increase to ∼100 bar, before stabilizing at pressures greater than 100 bar. Botto et al.[39] and Chiquet et al.[40] also carried out tests with quartz and brine and found a similar increase in the contact angle with increases in pressure. It is generally accepted that the contact-angle change is due to CO_2 adsorption/adhesion to the quartz surface,[41,42] and it has been suggested that flooding with CO_2 can be used as a mechanism to change the wettability of a rock sample from water-wet to mixed-wet. Dickson et al.[43] found that, although the effect diminished,

Downloaded from pubs.acs.org/enfuem/article-pdf/40/39/21742/6856715/acs.energyfuels.6c02931.pdf by TU DELFT user on 12 October 2026

https://doi.org/10.1021/acs.energyfuels.6c02931
Energy Fuels 2026, 40, 21742−21758

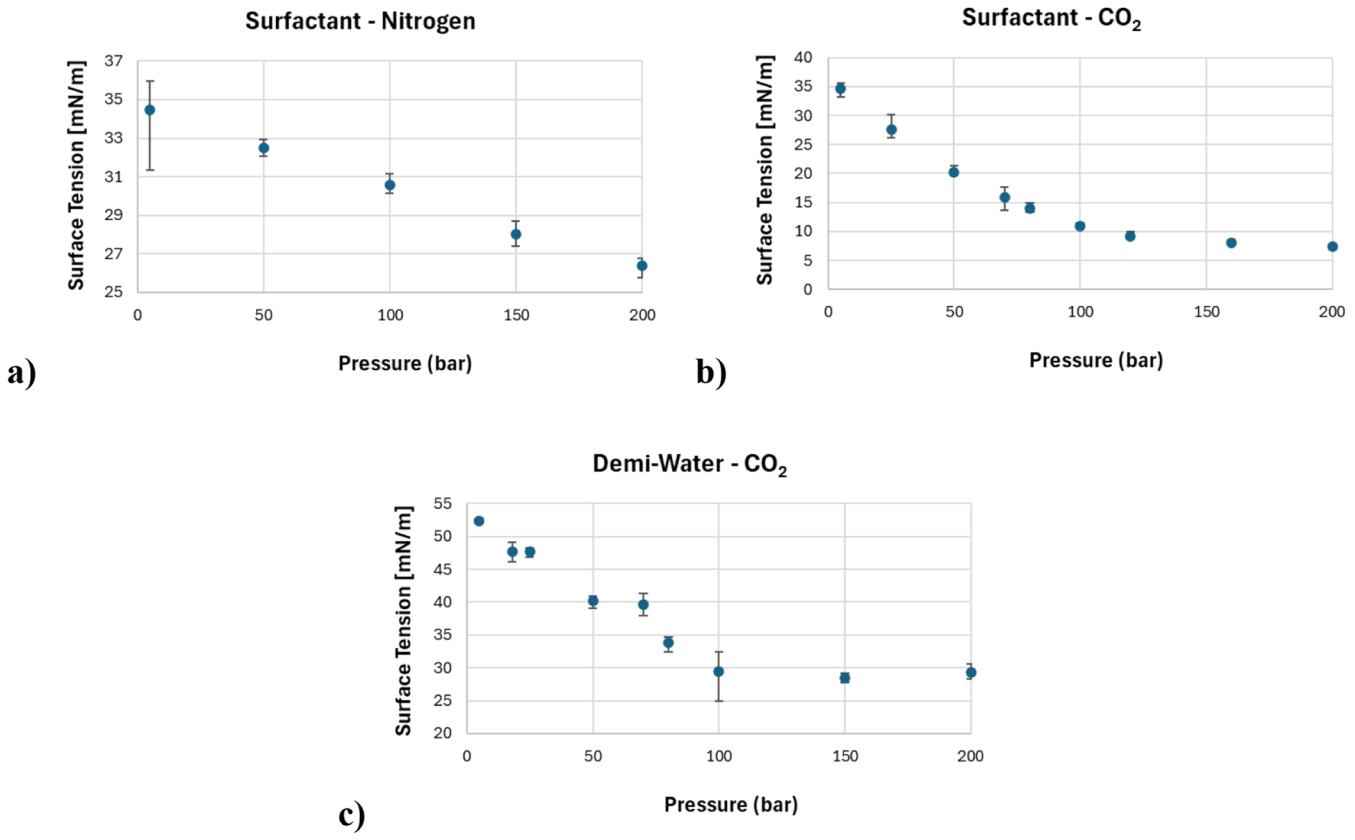

Figure 3. Variation in surface tension with pressure at 60 °C °C for a) surfactant solution and nitrogen, b) surfactant solution and CO_2, and c) demi-water and CO_2.

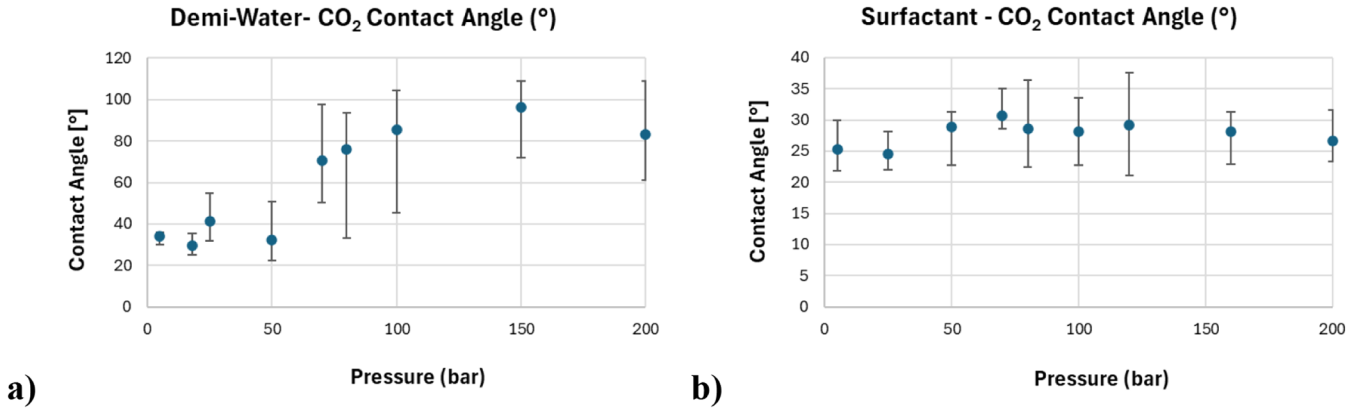

Figure 4. Contact angle measurements for quartz and CO_2 at 60 °C with a) demi-water and b) surfactant solution.

the wettability change persisted after the system was depressurized, and it was only after a week that the contact angles returned to pre-CO_2 flooding values.

In contrast, the contact angle measurements with the surfactant solution (Figure 4b) were consistently water-wet, even at the highest pressures tested. It is suggested that the wettability alteration by the surfactant adsorption[44] was the dominant effect, as compared to the CO_2, at least over the short time scale of the contact angle measurements.

Coreflood Tests—Nitrogen Foam

The foam quality scans obtained for the nitrogen foam tests, for both the midsection (dP2) and outlet (dP3) sections of the core, are presented in Figure 5 and Figure S1 (in Supporting Information), respectively. One test was carried out at each pressure except for 5 bar, where a repeat was carried out. For both the midsection and the outlet, the final gas flow velocities (and foam qualities) were calculated using the midpoint pressure for each section to determine the local density (and solubility) of the gas. Even when considering a steady-state pressure drop, there are fluctuations in the pressure measurements (as seen in Figure 9), and the error bars shown in the foam quality scans are calculated from the standard deviations of the pressure-drop fluctuations. There are generally larger fluctuations in the pressure measurements and, hence, larger error bars, at higher foam qualities.

As can be seen in Figure 5, there was good repeatability of the nitrogen foam-quality scans at the mid-range pressures of 50, 100, and 150 bar. As expected,[45] there was a small increase in

Downloaded from pubs.acs.org/enfuem/article-pdf/40/39/21742/6856715/acs.energyfuels.6c02931.pdf by TU DELFT user on 12 October 2026

https://doi.org/10.1021/acs.energyfuels.6c02931
Energy Fuels 2026, 40, 21742−21758

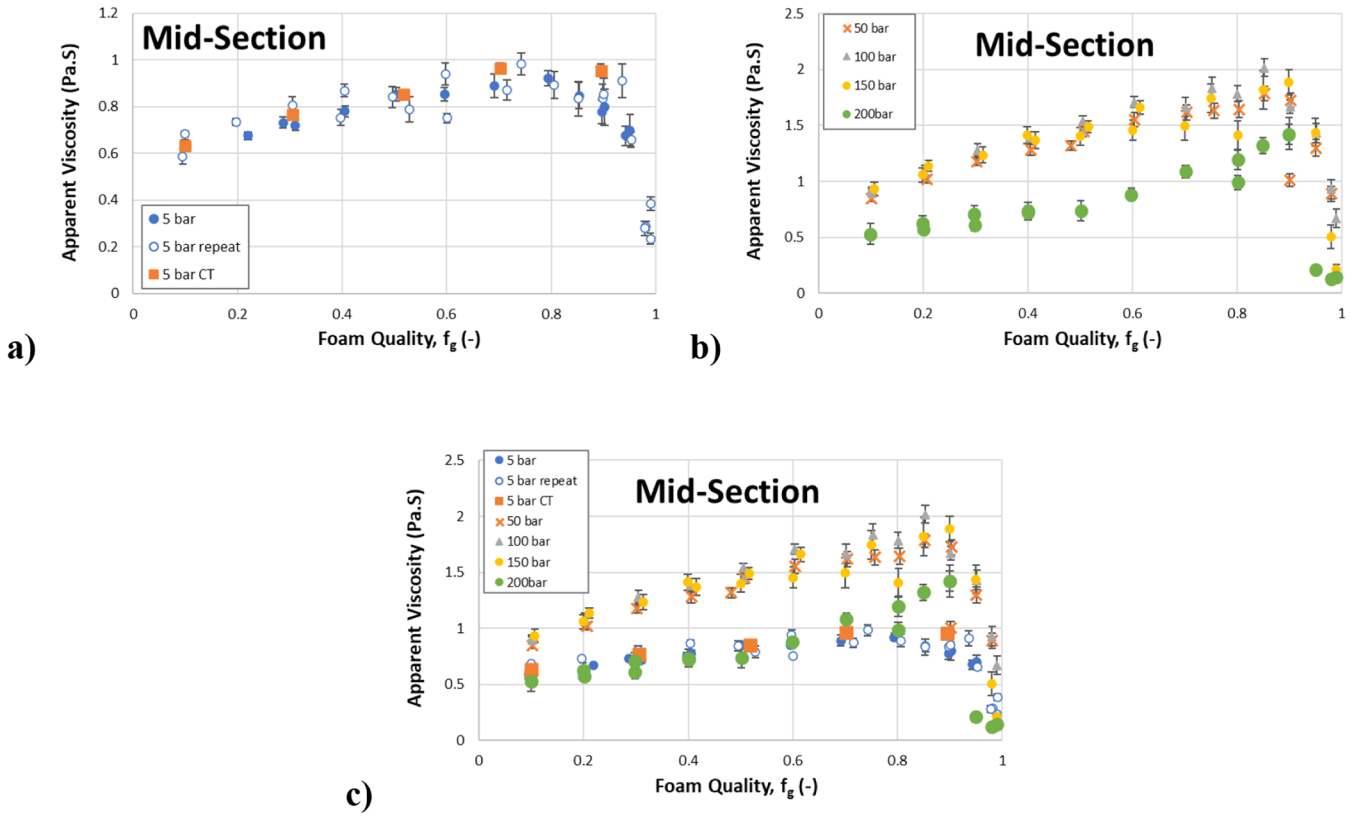

Figure 5. Foam-quality scans for nitrogen obtained using the pressure drops at the midsection (dP2) of the core. The three graphs show a) the behavior for the three tests carried out at 5 bar, b) the behavior at the higher test pressures, from 50 to 200 bar, and c) the data for all the test pressures shown together. The error bars are calculated from the standard deviation of the pressure-drop fluctuations observed at steady state and give an indication of the noise in the measurement.

maximum foam apparent viscosity with increasing system pressure, and this variation is most noticeable at the outlet of the core, as seen in Figure S1 and Table 4. However, in the midsection of the core, there was an unexpected reduction in the measured viscosities at both 5 and 200 bar.

Table 4. Summary of the Maximum Apparent Viscosity, $\mu_{app,max}$, and Transition Foam Quality, f_g*, for the Midsection and Outlet of the Core, at the Different System Pressures Tested for Nitrogen Foam

System Pressure (bar)	Maximum Measured Apparent Viscosity in Midsection (Pa·s)	f_g* for Midsection (−)	Maximum Measured Apparent Viscosity in Outlet (Pa·s)	f_g* for Outlet (−)
5	0.985	0.74	0.932	0.95
50	1.784	0.85	1.772	0.91
100	2.016	0.85	2.134	0.91
150	1.885	0.90	2.241	0.90
200	1.422	0.90	2.312	0.90

At 5 bar the apparent viscosities for the midsection of the core were reduced across the whole of the foam-quality scan, with a maximum foam apparent viscosity of ∼1 Pa·s, about half of the maximum of 2 Pa·s measured at 100 bar. The pressure gradient corresponding to the viscosity of 1 Pa·s is approximately 55 bar/m in the 2.7 D core-plug used for the 5 bar test. This corresponds to a pressure drop of ∼2.2 bar across the midsection of the core and ∼3.9 bar across the outlet. Thus, for the tests with 5 bar back-pressure, the effect of gas expansion along the core would be significant. Although attempts are made to take this gas expansion into account during pretest flow-rate calculations, the expansion could induce localized shear-thinning behavior that reduced the measured foam viscosity.

At 200 bar, the behavior in the midsection of the core was more complex. At lower foam qualities, the measured apparent viscosities were similar to those found at 5 bar, while at higher foam qualities the values of apparent viscosity began increasing toward the values seen at 150 bar (Figure 5b). The definitive reason for this behavior at 200 bar is not known, but it is possible that the foam-generation zone has extended into the middle section of the core at this pressure. This is made more likely due to the fact that the inlet section is shorter (5.5 cm) in the high-pressure setup used for the 200 bar tests as compared to the inlet (6.35 cm) in the lower-pressure setup (see Figures 1 and 2). The extension of the foam-generation zone into the middle section of the core would mean that the foam had not reached its full strength until after it had passed the P2 location. This would result in lower measured pressures, and hence lower calculated viscosities, in the midsection of the core. In contrast to the behavior in the midsection, at the outlet of the core the nitrogen foam shows the highest maximum apparent viscosity at 200 bar (Figure S1), continuing the trend of increasing foam strength with increasing test pressure (Table 4). The fact that the foam behaves differently between the midsection of the core and the outlet at 200 bar is probably due to 1) the foam finally reaching full strength before the outlet section of the core, if the foam generation zone had extended into the midsection as suggested above, and 2) capillary snap-off, a mechanism by which additional foam is generated at the exit of the rock core,[46]

Downloaded from pubs.acs.org/enfuem/article-pdf/40/39/21742/6856715/acs.energyfuels.6c02931.pdf by TU DELFT user on 12 October 2026

https://doi.org/10.1021/acs.energyfuels.6c02931
Energy Fuels 2026, 40, 21742−21758

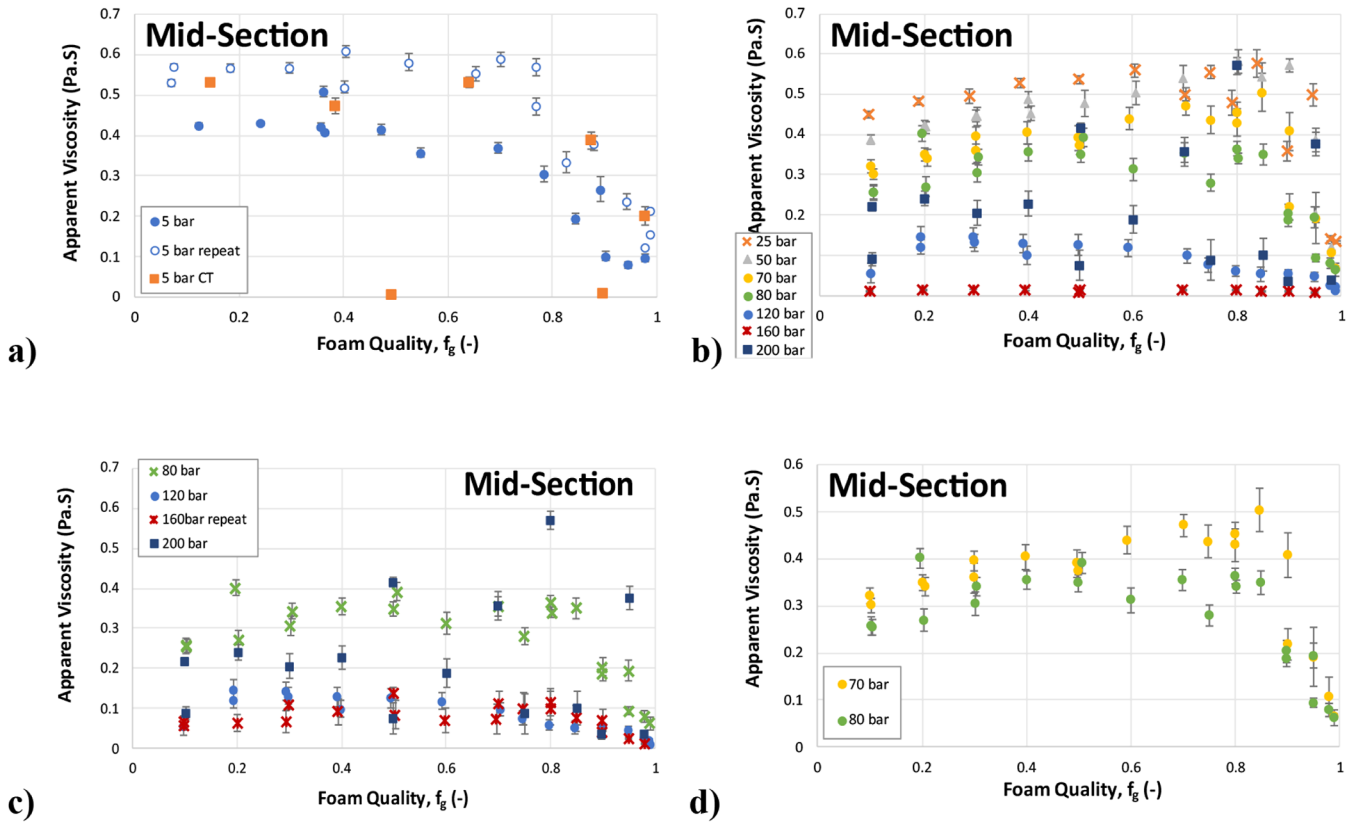

Figure 6. Foam-quality scans for CO_2 were obtained using the pressure drops at the midsection (dP2) of the core. The four graphs show a) the behavior for the three tests carried out at 5 bar, b) the behavior at all the higher pressures, from 25 bar up to 200 bar, c) a more-focused look at the behavior at the highest pressures, and d) the foam behavior around the supercritical transition. The error bars are calculated from the standard deviation of the pressure drop fluctuations observed at steady state and give an indication of the noise in the measurement.

which would help to maintain a strong foam at the outlet of the core even if there were the lower viscosities in the midsection.

Coreflood Tests—CO_2 Foam

The foam-quality scans for the CO_2 foam tests, for both the midsection and outlet section of the core, are presented in Figure 6 and Figure 8 respectively. For both sections of the core, the actual gas flow velocities (and foam qualities) were calculated using the midpoint pressure for each section to determine the local density of the gas and the CO_2 solubility into the brine. The error bars shown were again calculated from the standard deviations in the measured pressure drops.

CO_2 Foam Behavior in the Midsection of the Core

The foam-quality scans for all the tested pressures are presented in Figure 6. Contrary to the nitrogen behavior, the highest measured apparent viscosities were obtained with a system pressure of 5 bar (Figure 6a). However, the shape of the foam-quality scan was very unusual at this pressure, with the "low quality" part of the curve ($f_g < 0.7$) showing very little variation in apparent viscosity. This resulted in a curve that is close to horizontal, rather than the expected slope toward the origin. This could partly be due to the gas-expansion/shear-thinning effect suggested for the nitrogen foam at 5 bar. But it also suggests that the higher-than-expected viscosities measured in the low-quality regime are indicative of a high fraction of trapped gas within the core, which contributes to the low mobility of the foam by reducing the effective permeability of the gas moving through the rock.[47,48]

As the system pressure was increased, the maximum apparent viscosity did not increase (Table 5), as was observed for the nitrogen tests. Instead, the most noticeable effect of each increase in pressure was a decrease in the apparent viscosity over nearly the entire foam quality scan, with a simultaneous increase in the slope of the low-quality part of the curves. This change in slope indicates a change in the shear-thinning behavior of the foam.[29] At 25 bar, the slope in the low-quality region is small, indicating a high degree of shear-thinning, and there is a high viscosity at $f_g = 0.1$, which is again indicative of a large amount of trapped gas. Then, as the pressure increases, there is a strong

Table 5. Summary of the Maximum Apparent Viscosity, $\mu_{app,max}$, and Transition Foam Quality, f_g*, for the Midsection and Outlet of the Core, at the Different Tested System Pressures for CO_2 Foam

System Pressure (bar)	Maximum Measured Apparent Viscosity in Midsection (Pa·s)	f_g* for Midsection (−)	Maximum Measured Apparent Viscosity in Outlet Section (Pa·s)	f_g* for Outlet Section (−)
5	0.589	0.70	0.502	0.90
25	0.577	0.84	0.609	0.95
50	0.581	0.90	0.604	0.95
70	0.504	0.85	0.536	0.90
80	0.364	0.80	0.571	0.90
120	0.146	0.19	0.471	0.80
160	0.138	0.50	0.437	0.80
200	0.571	0.80	0.578	0.95

https://doi.org/10.1021/acs.energyfuels.6c02931
Energy Fuels 2026, 40, 21742−21758

Downloaded from pubs.acs.org/enfuem/article-pdf/40/39/21742/6856715 8/acs.energyfuels.6c02931.pdf by TU DELFT user on 12 October 2026

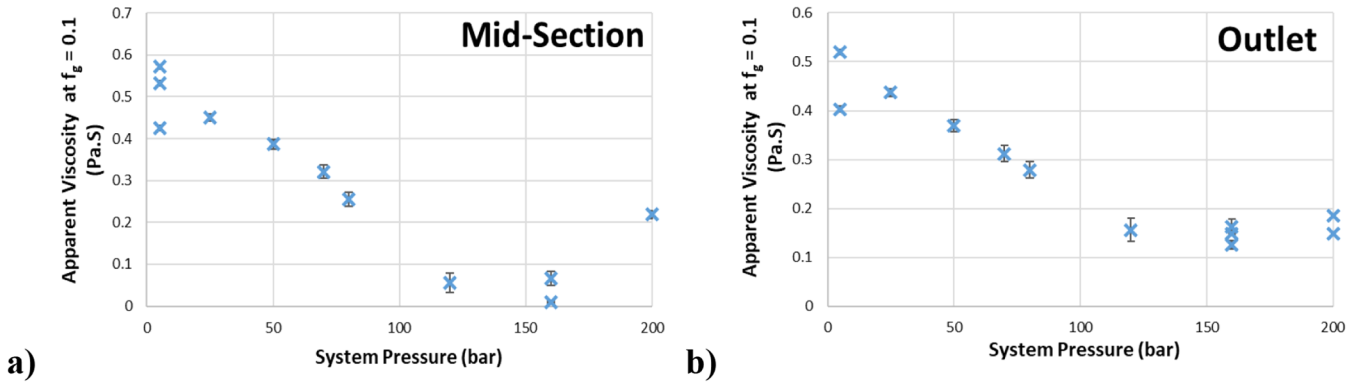

Figure 7. Variation in the measured apparent viscosity at $f_g = 0.1$ as a function of system pressure.

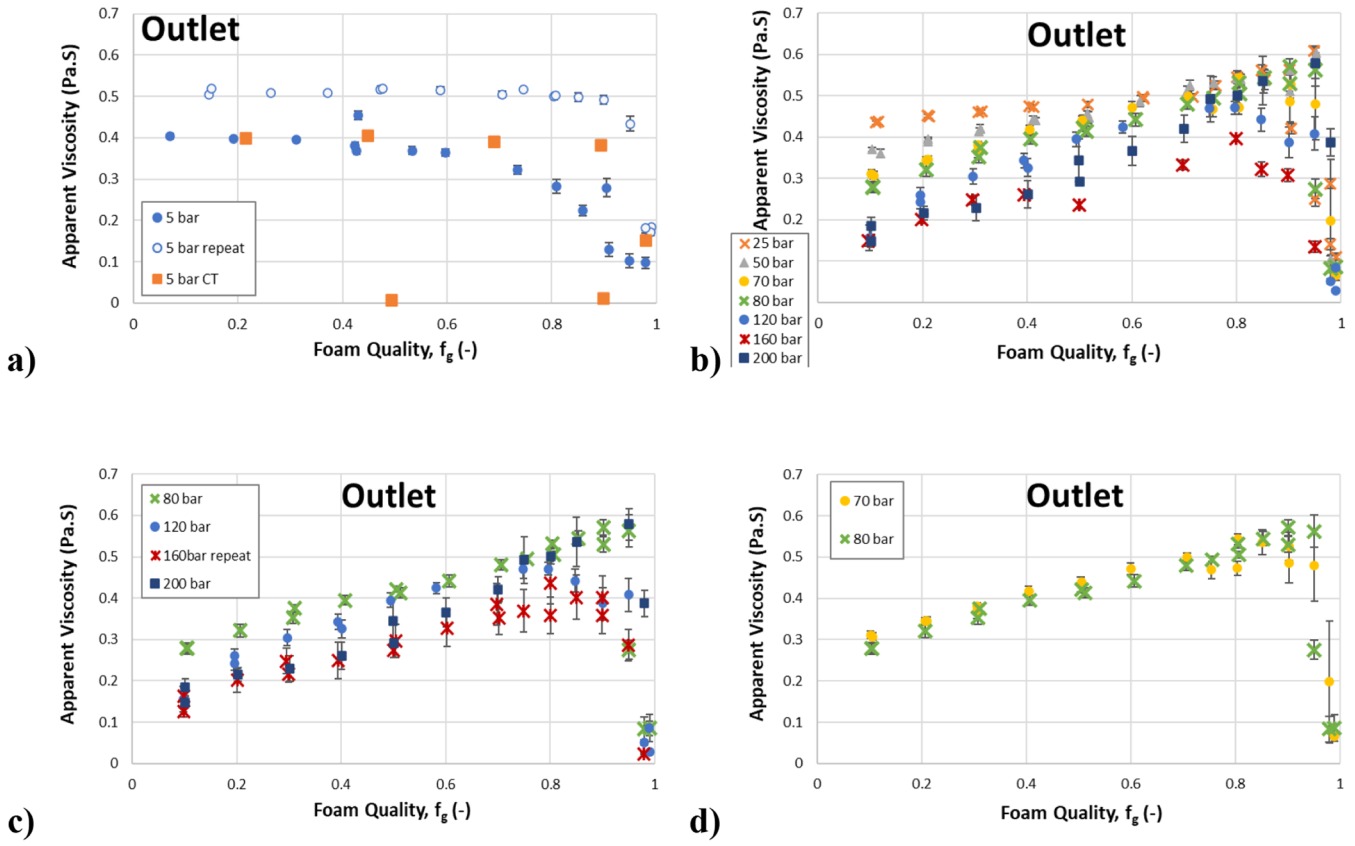

Figure 8. Foam-quality scans for CO_2 obtained using the pressure drop at the outlet section (dP3) of the core. The four graphs show a) the behavior for the three tests carried out at 5 bar, b) the behavior at all the higher pressures, from 25 bar up to 200 bar, c) a more-focused look at the behavior at the highest pressures, and d) the foam behavior around the supercritical transition. The error bars are calculated from the standard deviation of the pressure-drop fluctuations observed at steady state and give an indication of the noise in the measurement.

reduction in the apparent viscosity at $f_g = 0.1$ (Figure 7a), which suggests a reduction in trapped gas at higher system pressures. This suggestion is supported by 1) the knowledge that the IFT between CO_2 and a surfactant solution decreases significantly with increasing pressure, as measured above (and previously seen by multiple authors[35,42,49,50]). The lower IFT at high pressures makes it easier to remobilize foam films trapped in pore throats, thus reducing the quantity of gas trapped in the core; and 2) the experiments of Yu et al.,[51] where the authors found a step-change reduction (by a factor of >400) in the rate of coarsening between gaseous CO_2 (at 41 bar) and liquid (at 114 bar) or supercritical (at 152 bar) CO_2. Slower coarsening rates imply less trapped gas, as the lamellae will then take longer to migrate to minimal-energy configurations in the pore throats.

Finally, it should be noted that the results presented for 160 and 200 bar do not follow any of the general trends discussed above. The reason for this is discussed below in the "CO2 Foam: Challenges" section.

CO_2 Foam Behavior in the Outlet Section of the Core

The foam-quality scans for CO_2 foam at the outlet of the core for all the tested pressures are presented in Figure 8. The curves for the 5-bar tests show behavior in the low-quality regime that again indicates a large gas expansion along the core. For the higher-pressure tests, there was very little variation in the maximum measured apparent viscosity across all of the pressures

https://doi.org/10.1021/acs.energyfuels.6c02931
Energy Fuels 2026, 40, 21742−21758

Downloaded from pubs.acs.org/enfuem/article-pdf/40/39/21742/6856715 8/acs.energyfuels.6c02931.pdf by TU DELFT user on 12 October 2026

tested (Table 5). The biggest effect was again the changing gradient in the curves in the low-pressure regime, with the gradient increasing as the system pressure increased. This was accompanied by a drop in the apparent viscosity at $f_g = 0.1$, as shown in Figure 7b, likely due to changes in the trapped gas behavior (as discussed above).

In general, the foam scans at the outlet are less noisy than for the midsection, probably due to capillary snap-off at the end of the core,[45] which could help in maintaining the foam strength. This could be considered an artificial result. However, since many reservoirs are heterogeneous, with many transitions between low- and high-permeability rock where capillary snap-off could occur, these results are useful in showing the range of behavior that could be seen with a CO_2 foam.

Also, the difference between the results for the midsection and the outlet reinforces the importance of knowing how the foam behavior varies along the core. If the total pressure drop along the core (including the foam generation zone at the inlet) had been used to calculate the apparent viscosities, then the results would look quite different. Previously, Aarra et al.[17] tested the effect of varying system pressure (at $f_g = 0.8$) and found that CO_2 foam strength decreased significantly with an increase in system pressure, which would seem to contradict the current results. However, their work considered the pressure drop over the whole of the core, and the reality, as seen in the work here, may be that the foam behavior is more nuanced when the different regions of the core are treated separately and when the CO_2 foaming problems (discussed below) are taken into account.

CO_2 Foam: Challenges

Problems Observed at High Pressure. As can be seen in Figure 6b, it was very difficult to form any foam in the midsection of the core for the first test that was carried out at 160 bar. The maximum apparent viscosity achieved was only 0.015 Pa·s, a value significantly lower than previous tests. Some foam was observed in the outlet region of the core (Figure 8b), but the curve did not fit well with any of the previously observed trends. Because of the difficulty forming foam at 160 bar, the system pressure was reduced to 120 bar, where reasonable foaming behavior had previously been observed. However, this did not result in an improvement in the foaming behavior. It therefore appeared that the foaming problem might be related to a problem with the core, although there was no indication of any permeability change and no indication of any fouling at the inlet face of the core.

A new, fresh Bentheimer core was then placed in the setup. On restarting the tests with the new core, a test pressure of 200 bar was selected, as this was the maximum pressure in the test series. The foam-generation test at $f_g = 0.5$ (Figure 9) resulted in the very rapid generation of strong foam in the core. However, after a short period of time (~4 PV of injection) the pressure drop at the inlet of the core began to decrease, indicating that foam generation there was not completely stable. This effect of decreasing pressure drop and weakening foam at the inlet continued through the tests, and for this reason the duration of each foam-quality step was kept relatively short to try and minimize this effect.

After calculating the apparent viscosities for the test, the effect of the decreasing pressure at the inlet became obvious. As can be seen in Figure 10a, where the order of testing is indicated by the red numbers next to the data points, reasonable values of foam viscosity were obtained at the inlet of the core for the first three foam qualities tested. The apparent viscosities then decreased

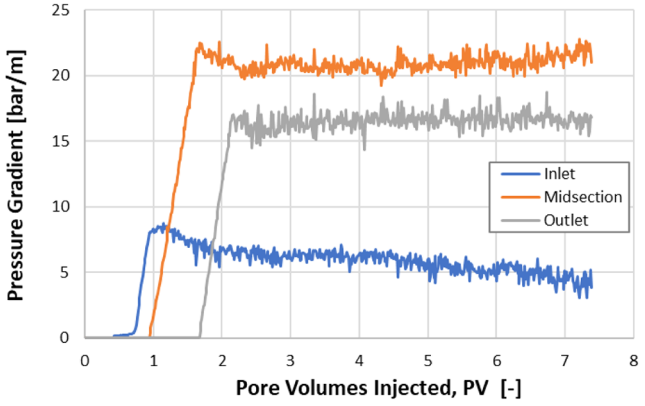

Figure 9. Foam-generation curves at 200 bar for the initial test at $f_g = 0.5$, showing strong foam generation within the core, beginning at the inlet.

significantly before stabilizing after the 5th data point, with values in the region of 0.01−0.02 Pa·s. This implies that some process is occurring that causes changes to the foam strength within about 1 day of the start of testing.

This decrease in foam strength is also seen in the midsection of the core, with a slower onset and a less rapid rate of decline in the apparent viscosity. Considering the graph in Figure 10b, it can be seen that the reduction in apparent viscosity began with small changes for data points 7 to 9. As the test progressed further, the apparent viscosity reduced significantly, with the data points from 12 onwards showing measured values of less than 0.1 Pa·s.

Following the test with the new core at 200 bar, the system pressure was dropped to 160 bar to repeat the foam flood at this pressure. Figure 11 shows the variation in foam behavior in the midsection of the core, between the new core and the previous core. The measured apparent viscosities with the new core were found to be significantly higher than those in the test with the old core but still with significantly lower magnitudes than the values measured initially in the fresh core at 200 bar.

Possible Reasons for the Foaming Problems Observed at High Pressure

Currently, there is no definitive reason for the changing behavior of the foam at the higher pressures. However, we suggest that there are four factors that influence the behavior—either individually or in combination.

1) ***High CO_2 density***: The density of the supercritical CO_2 at 200 bar is 0.726 g/mL,[20] which is very close to the density of the surfactant solution. It is suggested that this small density difference between the two phases can affect the foam behavior at the highest test pressures.
2) ***Surface tension variation with pressure***: As shown earlier, the surface tension of CO_2 and brine varies strongly with pressure. Although it is known that low surface tension can influence gas trapping and remobilization (as discussed above), it is not known to what extent foam generation and propagation are affected by the lower values of surface tension at higher test pressures. However, a lower surface tension, γ, implies a lower capillary pressure p_c (i.e., the difference in pressure between the gas and liquid phases defined as $p_c = 2\gamma/R$, where R is the radius of the curvature of the interface between the two phases), which in turn implies thicker

Downloaded from pubs.acs.org/enfuem/article-pdf/40/39/21742/6856715/acs.energyfuels.6c02931.pdf by TU DELFT user on 12 October 2026

https://doi.org/10.1021/acs.energyfuels.6c02931
Energy Fuels 2026, 40, 21742−21758

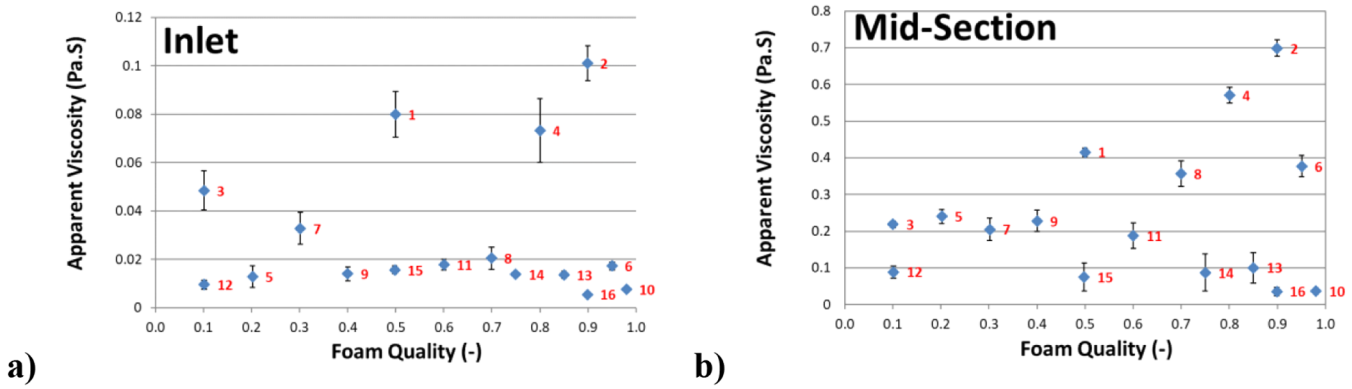

Figure 10. Apparent viscosities at a) the inlet and b) the middle section of the core during the 200-bar test with a newly placed Bentheimer core. The order of testing is indicated by the red numbers by each data point.

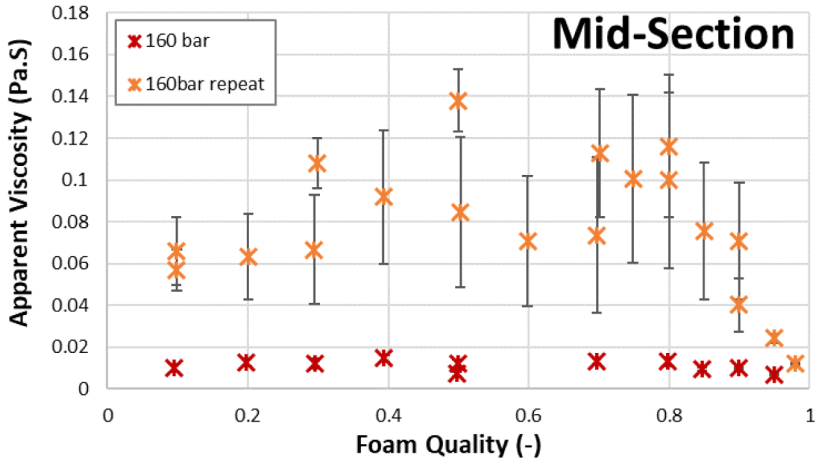

Figure 11. Variation in behavior between an "old" and "newer" core for CO_2 foam at 160 bar.

Plateau borders and the potential for changing flow behavior.

3) ***CO_2 chemistry affecting surfactant behavior***: The CO_2 content in the brine increases as pressure increases due to the increased solubility.[21] This increased CO_2 content will in turn cause the pH to decrease and the ionic state of the brine to change, which could then impact foam film stability.[52]
4) ***Supercritical CO_2 can affect rock wettability***: Probably the most significant factor is the fact that high-pressure CO_2 can have a significant effect on the CO_2-brine-rock contact angles, as shown in Figure 4a. Any changes in rock wettability have the potential to significantly impact foam generation[53] and propagation. In particular, any reduction in the water-wetness has the potential to destabilize foams, as Rossen[54] states, "*Foams are not expected to be stable in porous media that are not strongly water wet*" due to the increased likelihood of the bubble films becoming detached from the walls of the pores.

Considering this last point, we note that our corefloods contain surfactant, not brine, and it could be assumed that the surfactant adsorption onto the rock surface keeps the rock strongly water wet (Figure 4b). However, in our corefloods, the surfactant adsorption on the rock occurs during the early stages of each coreflood test before the injection of the CO_2. When there is continuous flow of high-pressure CO_2 through the core over multiple days, the adsorption of the CO_2 might begin to compete against the already adsorbed surfactant. This could potentially reverse the effect of the surfactant wettability change, gradually shifting the system toward less water-wet. This would provide an explanation for the gradual degradation of foam strength with time, as the core became slowly less water-wet, and why repeat tests in the same core also seem to show poor foaming behavior. This effect would not be reflected in Figure 4b, where the rock sample is fully saturated by the surfactant solution in the pendant-drop cell and where each data point was obtained after a relatively short time (<10 min) of exposure to the CO_2 bubble due to the fast dissolution of the CO_2 into the surrounding brine.

CT Scanner Tests

Two of the coreflood tests were carried out in the CT scanner to obtain information about the water saturation in the core during a foam flood. One test was carried out with CO_2 and one with nitrogen, both at a back-pressure of 5 bar.

CO_2 CT Scanner Tests

CO_2 Foam Tests. The foam tests were initiated at a foam quality of f_g = 0.5. CT scans were carried out at various stages during the foam-generation process −0.5 PV, 1.0 PV, 1.5 PV, 2.0 PV, and 33 PV; some of the resultant longitudinal images are shown in Figure 12. The associated saturation curves are then shown in Figure 13. Even though the foam generated at this point was not a strong foam, with measured μ_{app} < 10 mPa·S (see also the CT data in Figure 6a and Figure 8a), it still showed a relatively good sweep efficiency. However, the brine saturation in the core remained high, with a S_w of approximately 0.5.

Downloaded from pubs.acs.org/enfuem/article-pdf/40/39/21742/6856715/acs.energyfuels.6c02931.pdf by TU DELFT user on 12 October 2026

https://doi.org/10.1021/acs.energyfuels.6c02931
Energy Fuels 2026, 40, 21742−21758

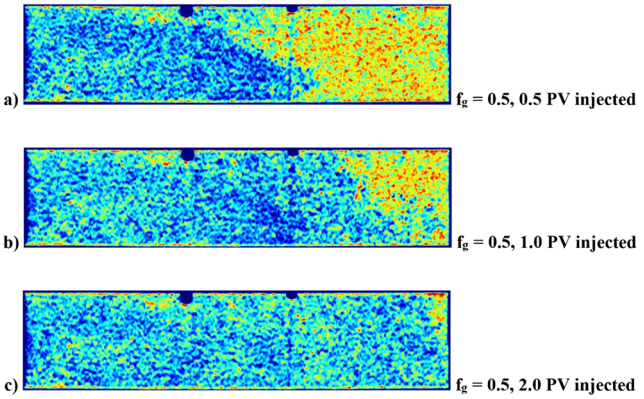

Figure 12. CT scans obtained during the generation of CO_2 foam at f_g = 0.5. Longitudinal slices of the core showing the regions of qualitatively higher (red) and lower (blue) brine saturation for a) 0.5 PV, b) 1.0 PV, and c) 2.0 PV injected.

The transition from the initially weak foam to a strong foam was triggered by an increase in the total flow rate in the system. Once a strong foam was initiated, the total flow rate was then returned to 1 mL/min, and CT scans were carried out at a range of foam qualities. The steady-state saturation profiles for the six tests carried out are given in Figure 14. The most noticeable features of the profiles are that 1) the water saturations are significantly lower than for the weak foam (Figure 13), 2) there is a spike in water saturation at the outlet of the core due to the capillary end effect, and 3) the water saturation is higher across the inlet section, with the measured S_w increasing as the gas fraction reduces. This last effect is likely a result of some of the CO_2 still being in solution (due to higher solubility) at the higher pressures at the inlet. The reduction in water saturation across the inlet section could then indicate the degassing of the CO_2 as the pressure drops along the core, and this is especially noticeable for the f_g = 0.1 test.

Considering the region of the core where the brine saturation is relatively constant (between 10 and 15 cm), it can be seen that the injected foam quality has a significant effect on S_w. The saturation decreases as the foam quality increases from a saturation of 0.2 at f_g = 0.1 to a saturation of approximately 0.09 at f_g = 0.98.

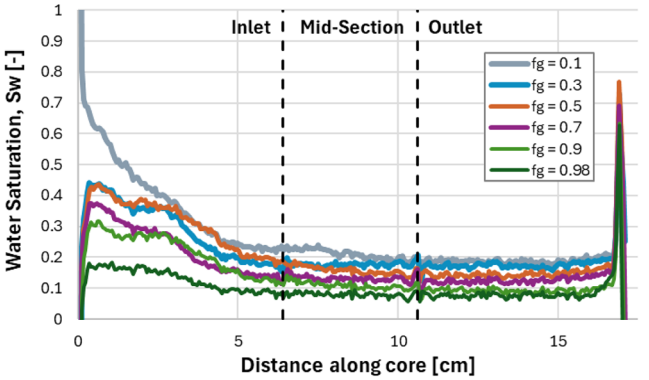

Figure 14. Saturation profiles for the steady-state CO_2 foam, showing the longitudinal variation in brine saturation for the six foam qualities tested. The dashed, vertical lines show the locations of the pressure sensors and indicate where the Inlet, Midsection, and Outlet apparent viscosity measurements were made.

Nitrogen CT Scanner Tests

For the nitrogen tests, a strong foam was very easily generated, and the saturation profiles for the five different foam qualities tested are shown in Figure 15. In comparison with the CO_2

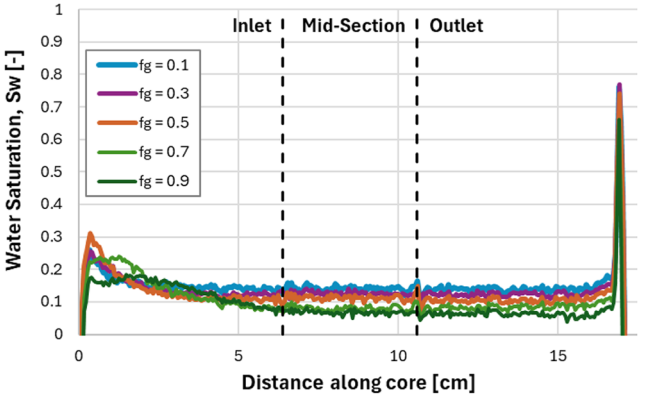

Figure 15. Saturation profiles for the steady-state N_2 foam, showing the longitudinal variation in brine saturation with the five foam qualities tested. The dashed, vertical lines show the locations of the pressure sensors and indicate where the Inlet, Midsection, and Outlet apparent viscosity measurements were made.

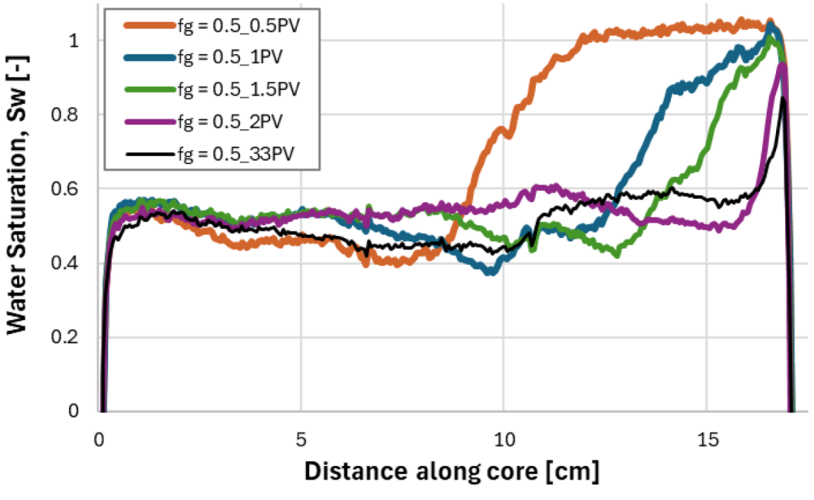

Figure 13. Saturation profiles for the CO_2 foam-generation test, showing the variation in S_w with pore volumes injected.

Downloaded from pubs.acs.org/enfuem/article-pdf/40/39/21742/6856715/8/acs.energyfuels.6c02931.pdf by TU DELFT user on 12 October 2026

https://doi.org/10.1021/acs.energyfuels.6c02931
Energy Fuels 2026, 40, 21742−21758

results (Figure 14), it can be seen that, in general, the water saturations are lower. For the inlet region, we again see an accumulation of brine in the foam-generation zone but with significantly lower water saturations than seen with CO_2. However, the spike in saturation at the end of the core, caused by the capillary end effect, does not appear to be affected by the gas type.

Considering the region of the core where the brine saturation is relatively constant (between 6.5 and 15 cm), the saturation again decreases as the injected foam quality increases, dropping down to $S_w \approx 0.06$ at $f_g = 0.9$. The highest water saturation, S_w, is approximately 0.14 at $f_g = 0.1$, which is much lower than the $S_w \approx 0.2$ seen with the CO_2. This would indicate that the higher viscosity foams generated with the nitrogen (comparing Figures 5 and 6) give a more efficient sweep of the core than the CO_2.

Fractional-Flow Curves

Considering the data from the CO_2 foam and nitrogen foam CT tests, as well as a no-foam test where only brine and CO_2 were co-injected, fractional-flow curves (Figure 16) can be generated,

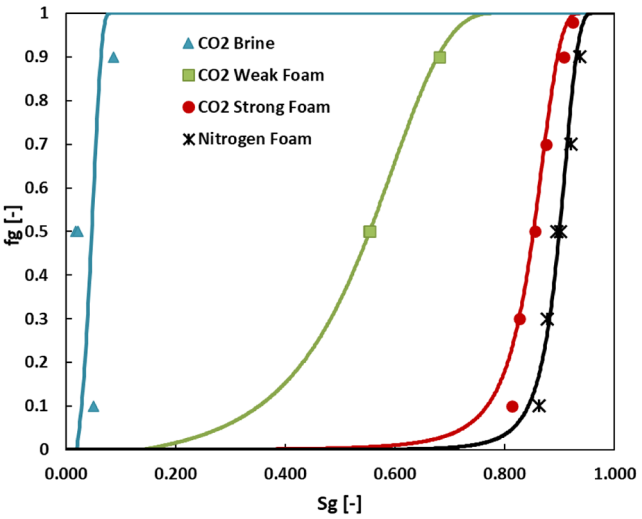

Figure 16. Fractional flow curves for CO_2 (no foam, weak foam, and strong foam cases) and nitrogen strong foam at 5 bar system pressure. The experimental data is represented by the markers, and the smooth lines give the model fit.

plotting injected f_g against S_g (= 1 − S_w). The value of S_w in each case was measured where there was no observable entrance or outlet effect, for distances along the core of 10−15 cm for the CO_2 tests and 6.5−15 cm for the N_2 tests. This experimental data can then be fitted using the fractional flow equations:[55]

$$f_g = \frac{1}{\left(1 + \frac{\mu_g}{\mu_w} \cdot \frac{k_{rwo}(1 - S_g^*)^{n_w}}{k_{rgo}(S_g^*)^{n_g}}\right)} \quad \text{where } S_g^* = \left(\frac{S_g - S_{gr}}{1 - S_{gr} - S_{wc}}\right)$$

Several of the variables—μ_g, μ_w, and S_{gr}—could be determined from the experimental data; then the values of n_w and n_g were tuned to ensure the best fit between the model curve and the data. The values of the parameters to give the best curve fits shown in Figure 16 are given in Table 6.

Fitting of Implicit-Texture Parameters

The Implicit-Texture parameters were fitted for the data sets at each pressure, and the full set of curve fits are given in Tables S3, S4, S5, and S6 (in Supporting Information). The parameter

Table 6. Fractional Flow Curve Fitting Parameters for the Curves in Figure 16

	S_{gr}	S_{wc}	n_g	n_w	μ_g	μ_w
CO_2−brine	0.02	0.92	0.938	2.46	1	0.467
CO_2 weak foam	0.14	0.22	0.938	2.46	4	0.467
CO_2 strong foam	0.03	0.06	0.938	3.1	600	0.467
Nitrogen strong foam	0.03	0.04	4	2.9	1000	0.467

values obtained are summarized in Figure 17 for the nitrogen foam tests and Figure 18 for the CO_2 foam tests. Data are shown for both the middle section and the outlet section of the core, as the foam-quality scans for both these regions could be quite different (e.g., Figures 6 and 8), especially at the higher pressure for the CO_2 foam tests. The parameters are plotted as a function of the system pressure to show the variation with pressure (if any) and to determine if there were any significant trends.

In general, the parameter plots are quite noisy, but this may be partly due to parameter interaction.[28,56] The data at 5 bar, for both gases and for both the original run and the repeat, was particularly difficult to fit because of the "flatter" nature of the data curve, and this gave the large variation in the obtained fitting parameters seen on the graphs for the 5 bar tests.

For the nitrogen results (Figure 17), there were some general trends observed in the fitting parameters with increasing pressure. Considering the results at both the midsection and the outlet of the core, there is some indication that as the pressure increases:

1. ***fmmob* is constant or increases**—In the midsection of the core, there was little variation in the values of *fmmob*, but the values at the outlet of the core showed an increase with pressure. This is as expected, since *fmmob* is defined as the maximum gas-mobility reduction and we would anticipate this variable to increase with increased maximum apparent viscosity. There is some noise in the values, but as discussed by Kapetas et al.,[56] there is parameter interaction among *fmmob*, *fmcap*, and *epcap*, so any small variations in the fit of the other variables could have influenced the trend in *fmmob*.
2. ***epdry* increases**—This reflects the fact that the transitions between the low and high foam quality regimes become sharper as the system pressure increases.
3. ***fmdry* is relatively constant**—This implies that S_w*, the water saturation at which the nitrogen foam collapses, remains fairly constant as pressure increases. The higher value of fmdry at 5 bar is related to the weaker foaming behavior observed at this pressure.

The CO_2 plots of the Implicit-Texture fitting parameters (Figure 18) were noisier than the nitrogen plots, reflecting the greater variation in the shapes of the CO_2 apparent viscosity curves. This meant that it was difficult to determine any strong trends in the fitting parameters with increasing pressure. However, considering the results at both the midsection and the outlet of the core, there is some indication that as the pressure increases:

1. ***fmmob* is relatively constant**—The values of *fmmob* in the midsection of the core showed little variation, apart from the 5 bar test, where the apparent viscosity curve was an unusual shape (Figure 8a). There was also a generally horizontal trend in the values for *fmmob* at the outlet of the core, but with greater scatter that could be partly attributed to parameter interaction.[56]

Downloaded from pubs.acs.org/enfuem/article-pdf/40/39/21742/6856715 8/acs.energyfuels.6c02931.pdf by TU DELFT user on 12 October 2026

https://doi.org/10.1021/acs.energyfuels.6c02931
Energy Fuels 2026, 40, 21742−21758

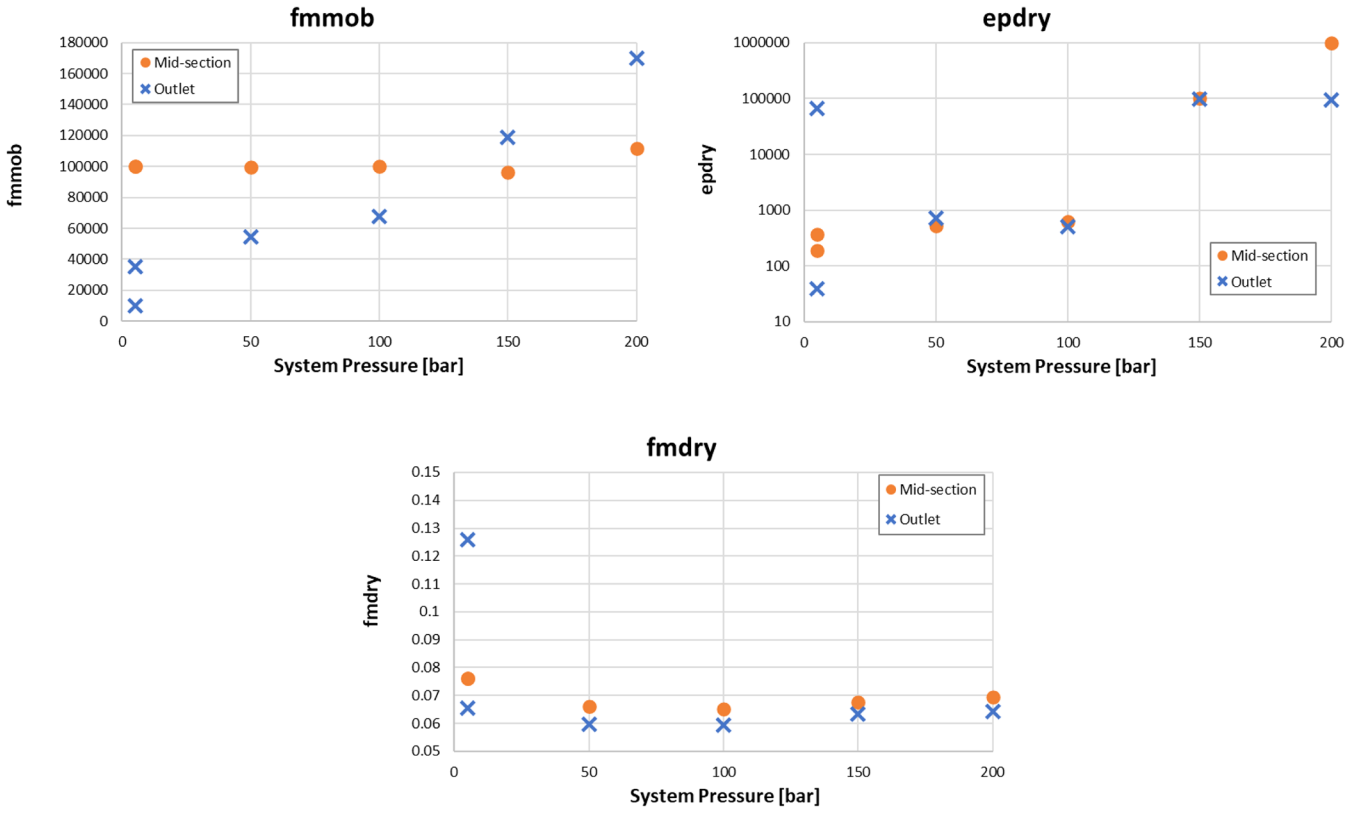

Figure 17. Implicit-Texture parameters plotted as a function of system pressure for the nitrogen foam for both the mid- and outlet sections.

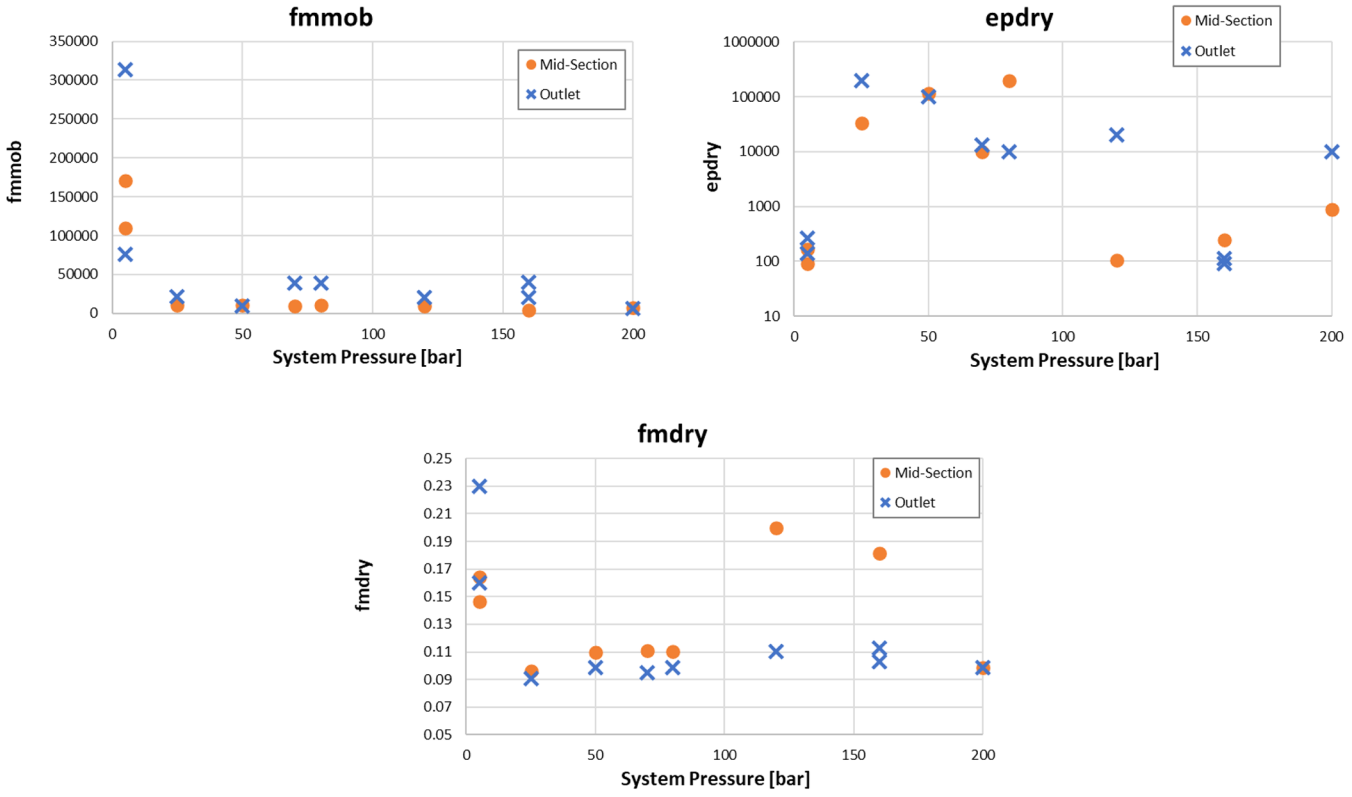

Figure 18. Implicit-Texture parameters plotted as a function of system pressure for CO_2 foam for both the mid- and outlet sections.

2. ***epdry*increases then decreases**—The transitions between the low and high foam-quality regimes initially become sharper as the pressure increases up to 80 bar, then become more rounded as the pressure continues to increase. The final data points at 200 bar reflect the initial foaming behavior observed in the fresh Bentheimer core,

https://doi.org/10.1021/acs.energyfuels.6c02931
Energy Fuels 2026, 40, 21742−21758

Downloaded from pubs.acs.org/enfuem/article-pdf/40/39/21742/6856715 8/acs.energyfuels.6c02931.pdf by TU DELFT user on 12 October 2026

where a sharper transition was seen during the first few tests in the new core (Figure 10b—where only data points 1 to 6 were used for the parameter fit).

3. ***fmdry* is relatively constant**—This implies that S_w*, the water saturation at which the CO_2 foam collapses, remains fairly constant as pressure increases. The main exception to this trend is again the data at 5 bar, but there were also some anomalous values in the midsection data at 120 and 160 bar. As discussed above, the CO_2 behavior becomes unusual at the higher pressures, with lower apparent viscosities being measured, and this could be linked to the observed higher values of S_w*.

CONCLUSIONS

A series of experiments have been carried out to test the variation in foam behavior in Bentheimer sandstone with system pressure. Tests were carried out with both nitrogen and CO_2 at pressures ranging from 5 bar up to 200 bar. In each test, a full foam-quality scan was carried out, measuring the foam apparent viscosity at injected foam qualities, f_g, from 0.1 to 0.99. The foam data obtained could then be fitted to obtain the implicit-texture foam model parameters required for future models. Two tests were also carried out in the CT scanner to obtain information on the water saturation, S_w, within the core during the foam tests.

Nitrogen Foam

- The nitrogen foam showed repeatable behavior with only minor changes between tests at different pressures. The only notable change was a small increase in the maximum apparent viscosity with an increasing system pressure.
- The exception to this trend is the result for the midsection of the core at 200 bar. The foam for this test showed significantly weaker behavior than was obtained for lower pressures. The reason for this is currently unknown, although it is possibly linked to the different pressure gauge locations in the high-pressure core holder, and the effect did not propagate to the outlet section of the core, where the expected strong foam was observed.
- The foam behavior at 5 bar showed low measured apparent viscosities due to large gas expansion/shear thinning along the core, but this behavior still fits with the trend of higher pressure giving higher maximum viscosities.

CO_2 Foam

- The CO_2 foam showed much more complicated behavior than nitrogen foam, with very different results between the midsection of the core and the outlet.
- For the CO_2 foam there was no trend of increasing maximum apparent viscosity with pressure, and in the midsection of the core the opposite was true, with the maximum apparent viscosities decreasing with pressure.
- The main effect of increasing the system pressure was to change the shape of the foam-quality scan curve at the lower foam qualities ($f_g < 0.6$). High measured viscosities at low foam quality are usually considered to indicate a large quantity of trapped gas in the core.[46,47] This suggests that the quantity of trapped gas decreases with increasing system pressure, an effect driven by the significant reduction in the surface tension between the CO_2 and the surfactant solution with pressure. The changing gradient of the foam-quality scan curve at $f_g < 0.6$ also indicates that the shear thinning behavior of the foam is changing.
- The changes in foam behavior in the midsection of the core, with foam strength gradually decreasing with both increasing system pressure and test duration, could be related to several issues. These include 1) CO_2 density changes; 2) surface tension changes, which affect gas trapping and capillary pressure; 3) changes in chemistry, due to dissolved CO_2, which can affect surfactant chemistry and foam film stability; and 4) changes in rock wettability due to CO_2 adsorption, which can affect both foam generation and foam stability if the rock becomes significantly less water-wet.

Of these four variables, it is suggested that the most significant, in terms of long-term foaming behavior at the highest pressures, is the change in rock wettability caused by the CO_2, which can cause a very significant drop in the achievable foam strength. However, this reduction in foam strength is potentially beneficial, as it is most likely to occur close to the wellbore, where weaker foam would give improved injectivity.

Implicit-Texture Model.

- The implicit-texture model parameters exhibited some general trends with varying system pressures, and the pressure variance of these fitting parameters should be taken into account when implementing the implicit-texture model within any reservoir simulator. For both the nitrogen and CO_2 foams, the value of *fmdry* was relatively constant with increasing pressure. In addition, the value of *fmdry* was lower for nitrogen, indicating a better stability at lower water saturations.
- For the nitrogen foam, *fmmob* was either constant or increased slightly, and *epdry* increased as the pressure increased.
- For the CO_2 foam, *fmmob* was constant with increasing pressure, but *epdry* showed both increasing and decreasing behavior, reflecting the complicated behavior of the CO_2 foam at the higher pressures.

Future Perspectives. As discussed in the introduction, this research is a step in understanding how foam behavior, and in particular CO_2 foam behavior, varies with pressure and why. Our results have shown that several variables are important in explaining the observed trends in foam behavior, in particular the variations in rock wettability and surface tension with pressure.

However, we acknowledge that there are still open questions remaining from this research, and we suggest that there are several avenues, looking forward, that require further research to resolve these open questions.

Wettability Alteration at High Pressure. We carried out basic measurements of contact angle for CO_2-quartz-brine and CO_2-quartz-surfactant at varying system pressures. However, the results in the presence of surfactant were not conclusive in explaining the effect on the core of long-term exposure to CO_2: the surfactant adsorption to the quartz surface kept the surface water-wet during the short lifetime of the CO_2 bubbles in the pendant drop cell. Measurements demonstrating the variation in contact angle with long-term exposure to high-pressure CO_2, along with surface characterization and surfactant adsorption measurements, would greatly improve the understanding of the observed CO_2 foam behavior at the highest pressures. Unfortunately, these measurements were outside the scope of the current project.

Downloaded from pubs.acs.org/enfuem/article-pdf/40/39/21742/6856715/acs.energyfuels.6c02931.pdf by TU DELFT user on 12 October 2026

https://doi.org/10.1021/acs.energyfuels.6c02931
Energy Fuels 2026, 40, 21742−21758

Physicochemical Properties of the Foam Films. No consideration was made of the basic foam film properties in this paper. However, knowledge of how properties such as film surface viscoelasticity, disjoining pressure, and interfacial rheology vary with pressure could potentially aid in the understanding of the overall foam behavior.

Application to Reservoir Models. The current work looks at the pressure response of foam in a homogeneous Bentheimer sandstone, but reservoir rocks are usually more complex in terms of rock structure and mineralogy. Reservoir brines are typically of much higher salinity and complexity than the simple brine used here.

1 In terms of rock structure, it is known that higher foam strengths are seen in higher-permeability rocks,[56] but also that a high degree of rock heterogeneity can mitigate this permeability effect.[19] The effect of permeability and heterogeneity on the pressure response is currently unknown; therefore, to determine the best implicit-texture foam parameters for use in a reservoir model, foam tests should be carried out in reservoir rock samples.

2 In terms of mineralogy, the current work looked at the response of a sandstone with high quartz content.[57] Previous work has also been carried out showing that CO_2 causes changes in wettability, from water-wet to non-water-wet, for several other rock types, including shale[58] and mica.[37] It is important that there be a good understanding of the wettability response of the reservoir rock to CO_2 when developing any reservoir model.

3 High brine salinity can affect the adsorption of the surfactant onto the rock surface[59] and reduce the solubility of CO_2 into the brine.[60,61] Both of these effects have the potential to impact the surface tension and/or the wettability change. Knowing the scale of any impact is important for any future reservoir model.

Implicit-Texture Model Fitting. The focus of the current work was to identify if there were any trends in the fitting parameters with varying pressure, and one can get an idea of the reliability of these trends from the scatter in the values. As mentioned above, foam corefloods in reservoir rocks at reservoir conditions would be necessary for obtaining the implicit-texture foam parameters for use in a reservoir model. In that case, it would be necessary to quantify the uncertainty in the fitting parameters to determine the degree of confidence in the parameters.

■ ASSOCIATED CONTENT

Supporting Information

The Supporting Information is available free of charge at https://pubs.acs.org/doi/10.1021/acs.energyfuels.6c02931.

Physical properties of nitrogen and CO_2 at 60 °C (Tables S1, S2); nitrogen foam-quality scans at the outlet of the core (Figure S1); complete STARS fit data for all the foam tests (Tables S3−S6) (PDF)

■ AUTHOR INFORMATION

Corresponding Author

Siân A. Jones − *Delft University of Technology, Delft 2628CN, The Netherlands;* orcid.org/0000-0002-2374-8391; Email: s.a.jones@tudelft.nl

Authors

Siavash Kahrobaei − *Shell Global Solutions International B.V., Amsterdam 1030BN, The Netherlands*

Jeroen Groenenboom − *Shell Global Solutions International B.V., Amsterdam 1030BN, The Netherlands*

William R. Rossen − *Professor Emeritus, Delft University of Technology, Delft 2628CN, The Netherlands*

Denis Voskov − *Delft University of Technology, Delft 2628CN, The Netherlands*

Rouhi Farajzadeh − *Delft University of Technology, Delft 2628CN, The Netherlands; Shell Global Solutions International B.V., Amsterdam 1030BN, The Netherlands;* orcid.org/0000-0003-3497-0526

Complete contact information is available at: https://pubs.acs.org/10.1021/acs.energyfuels.6c02931

Author Contributions

The manuscript was written through contributions of all authors. All authors have given approval to the final version of the manuscript.

Funding

We would like to acknowledge Shell Global Solutions International B.V. for the funding for this project.

Notes

The authors declare no competing financial interest.

■ ACKNOWLEDGMENTS

We would like to acknowledge all the technical laboratory support from Michiel Slob and the other technicians in the Reservoir Engineering lab at TU Delft for all their useful discussions and suggestions.

■ REFERENCES

(1) Batôt, G.; Fleury, M.; Nabzar, L. Study of CO_2 foam performance in a CCS context. In *Presented at the 30th International Symposium of the Society of Core Analysts*; Society of Core Analysts: Snowmass, 2016.

(2) Rossen, W. R.; Farajzadeh, R.; Hirasaki, G. J.; Amirmoshiri, M. Potential and challenges of foam-assisted CO_2 sequestration. *Geoenergy Sci. Eng.* **2024**, *239*, 212929.

(3) Bashir, A.; Abdulmoniem, M.; Gbadamosi, A.; Patil, S.; Aljawad, M. S.; Mahmoud, M.; Kamal, M. S. Application of Foam for Enhanced CO_2 Geological Storage: A Mini-Review. *Energy Fuels* **2024**, *38* (20), 19208−19221.

(4) Talebian, S. H.; Masoudi, R.; Tan, I. M.; Zitha, P. L. J. Foam assisted CO_2-EOR: A review of concept, challenges, and future prospects. *J. Pet. Sci. Eng.* **2014**, *120*, 202−215.

(5) Heller, J. P.; Lien, C. L.; Kuntamukkula, M. S. Foamlike Dispersions for Mobility Control in CO_2 Floods. *SPE J.* **1985**, *25*, 603−613.

(6) Enick, R. M.; Olsen, D.; Ammer, J.; Schuller, W.*Mobility and Conformance Control for CO_2 EOR via Thickeners, Foams, and Gels - A Literature Review of 40 Years of Research and Pilot Tests*; SPE, 2012

(7) Jian, G.; Fernandez, C. A.; Puerto, M.; Sarathi, R.; Bonneville, A.; Biswal, S. L. Advances and challenges in CO_2 foam technologies for enhanced oil recovery in carbonate reservoirs. *J. Petroleum Sci. Eng.* **2021**, *202*, 108447.

(8) Gozalpour, F.; Ren, S. R.; Tohidi, B. CO_2 EOR and storage in oil reservoir. *Oil Gas Sci. Technol.* **2005**, *60* (3), 537−546.

(9) Yu, Y.; Hanamertani, A. S.; Ahmed, S.; Jiao, Z.; McLaughlin, J. F.; Quillinan, S.Supercritical CO_2-foam screening and performance evaluation for CO2 storage improvement in sandstone and carbonate formations In *Abu Dhabi International Petroleum Exhibition & Conference*; SPE, 2021, .

Downloaded from pubs.acs.org/enfuem/article-pdf/40/39/21742/6856715/acs.energyfuels.6c02931.pdf by TU DELFT user on 12 October 2026

(10) Moradi-Araghi, A.; Johnston, E. L.; Zornes, D. R.; Harpole, K. J.Laboratory Evaluation of Surfactants for CO_2-Foam Applications at the South Cowden Unit, In *International Symposium on Oilfield Chemistry, Houston, TX*; SPE, 1997,
(11) Chang, S. H.; Grigg, R. B. Effects of foam quality and flow rate on CO_2-foam behavior at reservoir temperature and pressure. *SPE Reservoir Eval. Eng.* **1999**, *2* (3), 248−254.
(12) Rognmo, A. U.; Fredriksen, S. B.; Alcorn, Z. P.; Sharma, M.; Føyen, T.; Eide, Ø.; Graue, A.; Fernø, M. Pore-to-core EOR upscaling for CO_2 foam for CCUS. *SPE J.* **2019**, *24* (6), 2793−2803.
(13) Vieira, R. A. M.; Dos Santos, S. S. F.; Do Nascimento, L. P. T.; De Souza, D. M. P. T.; Da Silva, C. N.Experimental characterization to support a FAWAG project in an offshore pre-salt field, In *SPE Improved Oil Recovery Conference, Tulsa*; SPE, 2024.
(14) Hanamertani, A. S.; Elkhatib, O.; Yu, Y.; Ahmed, S.Innovative In-Situ Foam Generation and Injection Strategy Using Greenhouse Gases for Conformance Control, In *Abu Dhabi International Petroleum Exhibition and Conference, Abu Dhabi, UAE*; SPE, 2023.
(15) Kim, J. S.; Dong, Y.; Rossen, W. R.Steady-state flow behavior of CO_2 foam, *The SPE Improved Oil Recovery Conference, Tulsa, OK*; SPE, 2004, .
(16) Solbakken, J. S.; Skauge, A.; Aarra, M. G.Supercritical CO_2-Foam-The Importance of CO_2 Density on Foams Performance, *SPE Asia Pacific Enhanced Oil Recovery Conference, Kuala Lumpur, Malaysia*; SPE, 2013,
(17) Aarra, M. G.; Skauge, A.; Solbakken, J.; Ormehaug, P. A. Properties of N_2-and CO_2-foams as a function of pressure. *J. Pet. Sci. Eng.* **2014**, *116*, 72−80.
(18) Solbakken, J.*Experimental Studies Of N2-And CO2-Foam Properties In Relation To Enhanced Oil Recovery Applications*; PhD Thesis, University of Bergen, 2015, https://hdl.handle.net/1956/10110.
(19) Jones, S. A.; Kahrobaei, S.; Van Wageningen, N.; Farajzadeh, R. CO_2 foam behavior in carbonate rock: effect of surfactant type and concentration. *Ind. Eng. Chem. Res.* **2022**, *61*, 11977−11987.
(20) Lemmon, E. W.; Bell, I. H.; Huber, M. L.; McLinden, M. O. Thermophysical Properties of Fluid Systems. In *NIST Chemistry WebBook, NIST Standard Reference Database Number 69*, Linstrom, P. J.; Mallard, W. G., Eds.; National Institute of Standards and Technology: Gaithersburg MD. 2024.
(21) Duan, Z.; Sun, R.; Zhu, C.; Chou, I. An improved model for the calculation of CO_2 solubility in aqueous solutions containing $Na^+SO_4^{2-}$,K^+, Ca^{2+}, Mg^{2+}, Cl^-, and. *Mar. Chem.* **2006**, *98*, 131−139.
(22) Eftekhari, A. A.; Farajzadeh, R. Effect of foam on liquid phase mobility in porous media. *Sci. Rep.* **2017**, *7* (1), 43870.
(23) Huang, E.; Skoufis, A.; Denning, T.; Qi, J.; Dagastine, R. R.; Tabor, R. F.; Berry, J. D. OpenDrop: Open-source software for pendant drop tensiometry & contact angle measurements. *J. Open Source Softw.* **2021**, *6* (58), 2604.
(24) Xiao, Y.; Zheng, J.; He, Y.; Wang, L. Droplet and bubble wetting behaviors: The roles of surface wettability and roughness. *Colloids Surf., A* **2022**, *653*, 130008.
(25) Hashemi, L.; Boon, M.; Glerum, W.; Farajzadeh, R.; Hajibeygi, H. A comparative study for H_2-CH_4 mixture wettability in sandstone porous rocks relevant to underground hydrogen storage. *Adv. Water Res.* **2022**, *163*, 104165.
(26) *Computer Modeling Group (Calgary Alberta, Canada)*; STARS User's Guide, 2015.
(27) Cheng, L.; Reme, A. B.; Shan, D.; Coombe, D. A.; Rossen, W. R.Simulating foam processes at high and low foam qualities, In *SPE Improved Oil Recovery Conference, Tulsa, OK*; SPE, 2000
(28) Ma, K.; Farajzadeh, R.; Lopez-Salinas, J. L.; Miller, C. A.; Biswal, S. L.; Hirasaki, G. J. Non-uniqueness, numerical artifacts, and parameter sensitivity in simulating steady-state and transient foam flow through porous media. *Transp. Porous Media* **2014**, *102*, 325−348.
(29) Boeije, C. S.; Rossen, W. R. Fitting foam-simulation-model parameters to data: I. coinjection of gas and liquid. *SPE Reservoir Eval. Eng.* **2015**, *18* (2), 264−272.
(30) Kahrobaei, S.; Salazar, R. S. M. *Locally available MATLAB script*; TUDelft, 2018.
(31) Hebach, A.; Oberhof, A.; Dahmen, N.; Kögel, A.; Ederer, H.; Dinjus, E. Interfacial tension at elevated pressures measurements and correlations in the water+ carbon dioxide system. *J. Chem. Eng. Data* **2002**, *47* (6), 1540−1546.
(32) Tewes, F.; Boury, F. Thermodynamic and dynamic interfacial properties of binary carbon dioxide−water systems. *J. Phys. Chem. B* **2004**, *108* (7), 2405−2412.
(33) Bachu, S.; Bennion, D. B. Interfacial tension between CO_2, freshwater, and brine in the range of pressure from (2 to 27) MPa, temperature from (20 to 125) C, and water salinity from (0 to 334 000) $mg{\cdot}L^{-1}$. *J. Chem. Eng. Data* **2009**, *54* (3), 765−775.
(34) Bikkina, P. K.; Shoham, O.; Uppaluri, R. Equilibrated interfacial tension data of the CO_2−water system at high pressures and moderate temperatures. *J. Chem. Eng. Data* **2011**, *56* (10), 3725−3733.
(35) Amro, M.; Finck, M.; Jaeger, P.Foams at elevated pressure in EOR, In *SPE Middle East Oil and Gas Show and Conference, Manama, Bahrain*; SPE, 2015
(36) Chow, Y. F.; Maitland, G. C.; Trusler, J. M. Interfacial tensions of the (CO_2+ N_2+ H_2O) system at temperatures of (298 to 448) K and pressures up to 40 MPa. *J. Chem. Thermodyn.* **2016**, *93*, 392−403.
(37) Arif, M.; Al-Yaseri, A. Z.; Barifcani, A.; Lebedev, M.; Iglauer, S. Impact of pressure and temperature on CO2−brine−mica contact angles and CO2−brine interfacial tension: Implications for carbon geo-sequestration. *J. Colloid Interface Sci.* **2016**, *462*, 208−215.
(38) Ameri, A.; Kaveh, N. S.; Rudolph, E. S. J.; Wolf, K. H.; Farajzadeh, R.; Bruining, J. Investigation on interfacial interactions among crude oil−brine−sandstone rock−CO_2 by contact angle measurements. *Energy Fuels* **2013**, *27* (2), 1015−1025.
(39) Botto, J.; Fuchs, S. J.; Fouke, B. W.; Clarens, A. F.; Freiburg, J. T.; Berger, P. M.; Werth, C. J. Effects of mineral surface properties on supercritical CO_2 wettability in a siliciclastic reservoir. *Energy Fuels* **2017**, *31* (5), 5275−5285.
(40) Chiquet, P.; Broseta, D.; Thibeau, S. Wettability alteration of caprock minerals by carbon dioxide. *Geofluids* **2007**, *7*, 112−122.
(41) Dehghani, M. R.; Ghazi, S. F.; Kazemzadeh, Y. Interfacial tension and wettability alteration during hydrogen and carbon dioxide storage in depleted gas reservoirs. *Sci. Rep.* **2024**, *14* (1), 11594.
(42) Herring, A. L.; Sun, C.; Armstrong, R. T.; Li, Z.; McClure, J. E.; Saadatfar, M. Evolution of Bentheimer sandstone wettability during cyclic $scCO_2$-brine injections. *Water Resour. Res.* **2021**, *57* (11), No. e2021WR030891.
(43) Dickson, J. L.; Gupta, G.; Horozov, T. S.; Binks, B. P.; Johnston, K. P. Wetting phenomena at the CO_2/water/glass interface. *Langmuir* **2006**, *22* (5), 2161−2170.
(44) Noruzi, Y.; Sharifi, M.; Fahimpour, J.; Sabet, M.; Akbari, M.; Hosseini, S. The state-of-the-art of wettability alteration in sandstones and carbonates: A mechanistic review. *Fuel* **2024**, *356*, 129570.
(45) Holt, T.; Vassenden, F.; Svorstøl, I.Effects of pressure on foam stability; implications for foam screening, In *SPE Improved Oil Recovery Symposium, Tulsa, OK*; SPE, 1996
(46) Shah, S. Y.; Wolf, K. H.; Pilus, R. M.; Rossen, W. R. Foam generation by capillary snap-off in flow across a sharp permeability transition. *SPE J.* **2019**, *24* (1), 116−128.
(47) Lake, L. W. *Enhanced Oil Recovery*; Prentice Hall: New Jersey, 1988.
(48) Kovscek, A. R.; Radke, C. J. *Fundamentals of foam transport in porous media; No. DOE/BC-93000174*; Lawrence Berkeley National Lab: Berkeley, CA, United States, 1993. .
(49) Liu, Y.; Grigg, R. B.; Svec, R. K.*CO_2 foam behavior: Influence of temperature, pressure, and concentration of surfactan*; SPE: 2005.
(50) Fan, C.; Jia, J.; Peng, B.; Liang, Y.; Li, J.; Liu, S. Molecular dynamics study on CO_2 foam films with sodium dodecyl sulfate: Effects of surfactant concentration, temperature, and pressure on the interfacial tension. *Energy Fuels* **2020**, *34* (7), 8562−8574.
(51) Yu, W.; Zhou, X.; Kanj, M. Y. Microfluidic investigation of foam coarsening dynamics in porous media at high-pressure and high-temperature conditions. *Langmuir* **2022**, *38* (9), 2895−2905.

Downloaded from pubs.acs.org/enfuem/article-pdf/40/39/21742/6856715/acs.energyfuels.6c02931.pdf by TU DELFT user on 12 October 2026

https://doi.org/10.1021/acs.energyfuels.6c02931
Energy Fuels 2026, 40, 21742−21758

(52) Zeng, Y.; Farajzadeh, R.; Eftekhari, A. A.; Vincent-Bonnieu, S.; Muthuswamy, A.; Rossen, W. R.; Hirasaki, G. J.; Biswal, S. L. Role of gas type on foam transport in porous media. *Langmuir* **2016**, *32* (25), 6239−6245.
(53) Starnoni, M.; Pokrajac, D. Numerical study of the effects of contact angle and viscosity ratio on the dynamics of snap-off through porous media. *Adv. Water Resour.* **2018**, *111*, 70−85.
(54) *Foams: Theory, Measurements, and Applications*; Rossen, W. R.; Prud'homme, R. K.; Khan, S. A., ed.; Routledge, 2017; pp. 610.
(55) Lake, L. W.; Johns, R. T.; Rossen, W. R.; Pope, G. A. *Fundamentals of Enhanced Oil Recovery*; Society of Petroleum Engineers (SPE); 2014. .
(56) Kapetas, L.; Vincent Bonnieu, S.; Farajzadeh, R.; Eftekhari, A. A.; Mohd Shafian, S. R.; Kamarul Bahrim, R. Z.; Rossen, W. R. Effect of permeability on foam-model parameters: An integrated approach from core-flood experiments through to foam diversion calculations. *Colloids Surf., A* **2017**, *530*, 172−180.
(57) Peksa, A. E.; Wolf, K. H. A.; Zitha, P. L. Bentheimer sandstone revisited for experimental purposes. *Mar. Pet. Geol.* **2015**, *67*, 701−719.
(58) Kaveh, N. S.; Barnhoorn, A.; Wolf, K. H. Wettability evaluation of silty shale caprocks for CO_2 storage. *Int. J. Greenhouse Gas Control* **2016**, *49*, 425−435.
(59) Belhaj, A. F.; Elraies, K. A.; Mahmood, S. M.; Zulkifli, N. N.; Akbari, S.; Hussien, O. S. The effect of surfactant concentration, salinity, temperature, and pH on surfactant adsorption for chemical enhanced oil recovery: a review. *J. Pet. Explor. Prod. Technol.* **2020**, *10*, 125−137.
(60) Zhang, Y.; Lashgari, H. R.; Sepehrnoori, K.; Di, Y. Effect of capillary pressure and salinity on CO_2 solubility in brine aquifers. *Int. J. Greenhouse Gas Control* **2017**, *57*, 26−33.
(61) Sun, R.; Hu, W.; Duan, Z. Prediction of nitrogen solubility in pure water and aqueous NaCl solutions up to high temperature, pressure, and ionic strength. *J. Solution Chem.* **2001**, *30*, 561−573.

Downloaded from pubs.acs.org/enfuem/article-pdf/40/39/21742/6856715 8/acs.energyfuels.6c02931.pdf by TU DELFT user on 12 October 2026

https://doi.org/10.1021/acs.energyfuels.6c02931
Energy Fuels 2026, 40, 21742−21758